

Deterministic seismic hazard assessment of the area comprised between west Gulf of Cádiz and east Alboran Sea

Adrián José Rosario Beltré^{1,2}, Carlos Paredes Bartolomé¹, Miguel Llorente Isidro³

¹ Department of Geological and Mining Engineering, Higher Technical School of Mines and Energy, Universidad Politécnica de Madrid (UPM), Ríos Rosas 21, 28003 Madrid, Spain

² Department of Geological Resources for the Ecological Transition, Geological Survey of Spain (IGME), Spanish National Research Council (CSIC), La Calera 1, 28760 Tres Cantos (Madrid), Spain

³ Department of Geological Risk and Climatic Change, Geological Survey of Spain (IGME), Spanish National Research Council (CSIC), Rios Rosas 23, 28003 Madrid, Spain

Correspondence to: Adrián José Rosario Beltré (aj.rosario@igme.es) Carlos Paredes Bartolomé (carlos.paredes@upm.es)

Abstract. The convergence zone of the NE-SW complex at the Eurasian-Nubian plate boundary is frequently affected by seismic activity. This activity has caused moderate to high magnitude earthquakes and that may have triggered tsunamis either directly due to seabed elastic deformation or indirectly by triggering submarine landslides. Tsunami risk in the area is significant and increasing mainly because of the growing economic and social pressure on the coasts. Although seabed deformation after earthquakes in tsunami hazard has a de facto standard study approach, seismicity and submarine landslides are not well considered amongst different initiatives. To understand tsunamis caused by landslides, we need to consider both geomechanical properties and the spatial distribution of PGA (Peak Ground Acceleration) as a triggering mechanism. This paper is the first of a series of papers to follow, showing our stepwise approach towards better understanding seismic triggers of landslides that may cause tsunamis. In this paper we present a deterministic seismic hazard assessment (DSHA) preceding other approaches to be presented soon after. The idea behind testing different methods is to assess the advantages and disadvantages of each approach to be considered as an input in landslide susceptibility. Our main contribution to the DSHA approach is to include a full 3D model to estimate peak ground acceleration (PGA). The results show that significant accelerations can be expected in the marine area along with a notable varied spatial distribution. Hence it proves the need to further and better study the seismic effects on the seabed, which are usually blanked out in seismic hazard maps. This information is essential in the assessment of slope instabilities that may cause tsunamis.

1. Introduction

The area between the Gulf of Cádiz and the Alboran Sea (Ibero-Maghrebian region) is located on the Eurasian-Nubian plate boundary (Bufo et al., 2016). It comprises the southern Iberian Peninsula and the Maghreb (western part of North Africa) and its tectonics is medium to moderate active with frequent seismicity due to the convergence of the African and

Eurasian plates. Major and devastating earthquakes have also been registered in the area (Buforn et al., 2015) such as the
 35 1755 Lisbon earthquake and tsunami (Table 1).

Table 1: Location, date and magnitude of some large earthquakes in the Ibero-Maghrebian region.

Region	Location	Date	Magnitude	Casualties	Reference
Southern Iberian Peninsula	Málaga	10.09.1680	6.8	70	Goded et al. (2008)
	Lisbon	11.01.1755	7.7	100,000	Chester (2001), Fonseca (2020)
	Torre Vieja, Alicante	03.21.1829	6.8 - 6.9	389	Silva et al. (2019)
	Andalusian	25.12.1884	6.5 - 6.7	839	Udias and Muñoz (1979)
	Adra, Almería	16.06.1910	6.1	-	Stich et al. (2003)
	Cape St. Vincent, Portugal	28.02.1969	7.8	19	López Arroyo and Udías (1972)
North Africa	Orán, Algeria	09.10.1790	6.0 - 6.5	2,000	Ayadi and Bezzeghoud (2014)
	El-Asnam, Algeria	10.10.1980	7.3	2,633	Ayadi and Bezzeghoud (2014)
	Zemmouri, Algeria	21.05.2003	6.8	2,278	Ayadi and Bezzeghoud (2014)
	El-Hoceima, Morocco	24.02.2004	6.4	629	Tahayt et al. (2009)

Nowadays, the two broad standard approaches to Seismic Hazard Analysis (SHA) are Deterministic Seismic Hazard
 40 Analysis (DSHA) and Probabilistic Seismic Hazard Analysis (PSHA) (Reiter, 1990). These methods remain the most widely
 used in regional seismic hazard assessments worldwide (e.g., Loi et al., 2018; Sinha and Sarkar, 2020) although they have
 also been criticised (Castaños and Lomnitz, 2002; Kossobokov and Panza, 2022). Although, the approach offered by a
 probabilistic assessment PSHA is currently the most widely implemented by the scientific community in seismic hazard
 assessment and mitigation plans, the DSHA is still considered useful in "worst-case" scenario modeling situations (Grasso
 45 and Maugeri, 2012; Mostafa et al., 2019). The latter is an approach to hazard estimation commonly used by civil protection
 systems. DSHA was the first methodology proposed in the late 1960s to assess seismic hazard in nuclear power plant design
 and engineering projects and was later applied to large industrial infrastructures (NRC, 1973; AEIS-IGN, 1979). This
 method assumes that seismicity behaves stationary by assuming that future earthquakes will occur in a similar way as they
 did in the past. The simplicity of its application is based on the fact that the seismic information required for its
 50 implementation uses geology and seismic history to identify earthquake sources and interpret the strongest earthquake that
 each source is capable of producing, regardless of time, or maximum credible or capable earthquake (MCE) (Krinitzsky,
 2005). Therefore, the DSHA is a method that does not provide information on the return period of the MCE. The MCE
 earthquake is the largest possible occurrence along a recognised fault under currently known or assumed tectonic activity
 (USCOLD, 1995). However, it should be noted that DSHA and PSHA can complement each other, providing more
 55 information about the existing seismic hazard at the site under study (Wang et al., 2012).

The test area in this work has not been addressed in seismic hazard studies recently despite its significant record of earthquakes, submarine landslides and tsunamis (Rodríguez et al., 2017; Vázquez et al., 2022b). Moreover, the first and only attempt to assess the seismic hazard in this area was made by Molina Palacios (1998), in which the seismic hazard of the Iberia-Africa contact area was based on a probabilistic approach. However, no DSHA approaches have been carried out in this submarine region. The study area includes some emerged land: the coastal areas of the southern Iberian Peninsula and North Africa. These emerged sites do have exhaustive seismic hazard studies, using both deterministic and probabilistic approaches. Several studies have been conducted in the Iberian region (e.g., Crespo et al., 2014; Salgado Gálvez et al., 2015; IGN-UPM, 2017; Rivas-Medina et al., 2018) to assess seismic hazard using PSHA method. Recently Neo-deterministic Seismic Hazard Assessment (NDSHA) has been applied for the Iberian Peninsula (García-Fernández et al., 2022) and for Sevilla city (Sá et al., 2021). In the North African part, Poggi et al. (2020) performed a PSHA, and Mourabit et al. (2014) also conducted an NDSHA approach in this region.

The main goal of this paper is to fill the gap of studying the marine area between the W of the Gulf of Cádiz and the E of the Alboran Sea, using a DSHA approach. To carry out this analysis, we have used an improved and upgraded model from Wang et al. (2012). To test the reliability of the outcomes, we have compared our results in the emerged land with previous work carried out in those areas with other seismic hazard analysis techniques (e.g., NDSHA, PSHA). This work is the first DSHA carried out in the Ibero-Maghrebian submarine region.

2. Seismotectonic setting of the study area

The study region extends from 11.5°W to 2°E; from the Goringe Ridge and the Horseshoe Abyssal plain to the Algerian compression belt (Fig. 1). The northern edge is bounded from WNW to ESE at latitude 38°N, by the Algarve region to the Guadalquivir basin. This limit runs parallel to the ENE-WSW Cenozoic reverse fault line, along the southern boundary of the Guadalquivir depression with the Betic, parallel to the Crevillente fault, and its extension to Cabo de la Nao, close to the Don Juan fault, the beginning of the Valencia trough. To the south, it follows the trace of the Gibraltar transform fault WNW-ESE at latitude 34°N to the Rif region and from there it takes an ENE-WSW direction parallel to the Algeria's Mediterranean Coast along the southern boundary of the Atlas Mountains, parallel to Arzew faults, to the Algerian Ténés and Thenia faults systems.

The tectonic structures of this region are still active today as proven with seismic records. This activity is also demonstrated after geodetic data and geodynamic studies that have been carried out for decades (e.g., Buform et al., 1995, 2016; Soumaya et al., 2018). Tectonic models of NW-SE to WNW-ESE show oblique convergence between the Nubia and Iberian plates (Reilly et al., 1992; Herraiz et al., 2000) with displacements of 2 to 5 mm/yr (Nocquet, 2012) of the western Betic Cordilleras with respect to the Iberian Massif (Palano et al., 2013; Gonzalez-Castillo et al., 2015). The Gulf of Cádiz and Alborán Sea basins are characterized by a complex geodynamic context resulting from the interaction between tectonic

plates (Custódio et al., 2016; Neres et al., 2016). This area is highly active geologically, with moderate to low-moderate seismic activity. Historical cases have demonstrated the occurrence of such hazards in the region (Vázquez et al., 2022a). The plate boundary of the study area is usually divided into four main areas according to their stress regime: the SW as simple shear zone, the pure shear Gulf of Cadiz as the Eastern Betic, and the South Moroccan compressional arc.

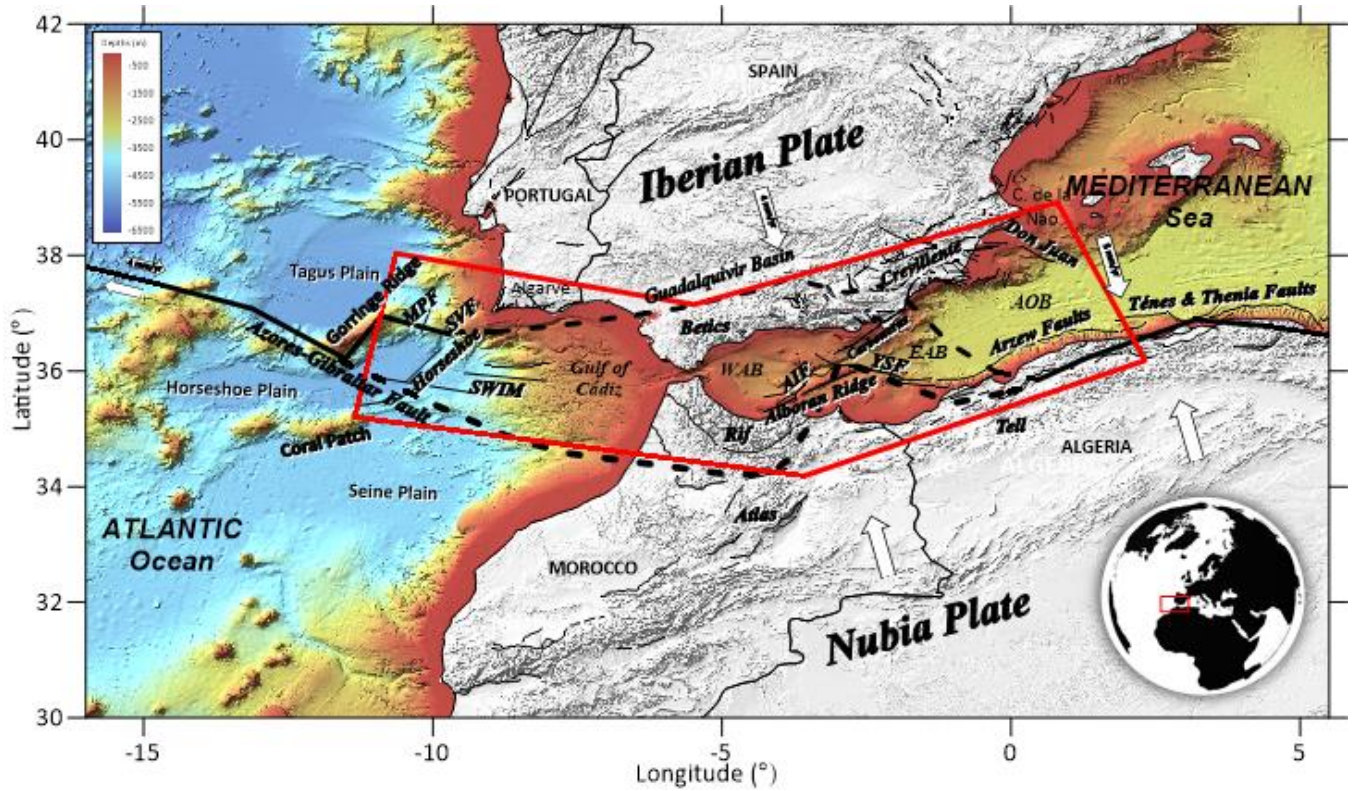


Figure 1. Location of the area of interest of this work in relation to the tectonic setting. Abbreviations are as follows: WAB: Western Alboran Basin, EAB: Eastern Alboran Basin, AOB: Algerian Oceanic Basin, SVF: Sao Vicente Fault, MPF: Marques de Pombal fault, SWIM: Southwest Iberian Margin lineaments (1, 2 and 3). AIF: Al Idrisi fault, YSF: Yusuf fault. Background: shadowed Digital Terrain Model (altimetry and coloured bathymetry) in the study area (extracted from GEBCO, 2020).

The Gulf of Cádiz is located on the contact boundary between the Eurasian and African plates. It extends from the Azores Islands to the Strait of Gibraltar, through the Iberian massif and the Algarve region to the north, and, in the eastern part, through the orogenic arc of the Betic-Rifeña mountain range. It is characterised by a NW-SE oblique convergence regime, mainly controlled by the formation of the Betic-Rifeño Orogen and by the accommodation of post-orogenic compressional tectonic activity (IGN, 2023). This tectonic configuration makes seismic activity in the Gulf of Cádiz significant, with moderately deep earthquakes ($h < 40 - 60$ km), but no subduction zone has been clearly marked (Custódio et

al., 2016). Some moderate magnitude earthquakes have also been recorded (Martín-Dávila and Pazos, 2003). Most of the
105 focal mechanisms in this area are reverse and rifting type. There is also historical and instrumental evidence of several high-
magnitude earthquakes in the region. These include the earthquakes of 1755 ($M_w \sim 7.7$; Mendes-Victor et al., 2009) and
1969 ($M_w \sim 7.8$; López Arroyo and Udías, 1972), both causing tsunamis that affected the coasts of Morocco, Portugal, and
Spain. The Gorringe Bank, the Sao Vicente submarine canyon (Sao Vicente fault), Horseshoe, Marqués de Pombal, and the
SWIM faults show the greatest seismicity in the region surrounded by the Gorringe Ridge, the Coral Patch, the Horseshoe
110 and Seine abyssal plains.

The Alboran Sea is the westernmost part of the Mediterranean Sea. It is bordered by the Alpine Mountain ranges of the
Betic, in the Iberian Peninsula and the Rif in the north of Africa. It is a complex contact zone between the Eurasian and
Nubian tectonic plates, whose genesis and evolution are related to the process of convergence between these plates, due to
the northward motion of the African plate. Among the tectonic structures, the submarine mountain ranges stand out, with a
115 length of more than 50 km, oriented NE-SW and delimited to the north and south by reverse faults with opposite dip. On the
other hand, there are two sets of conjugate directional faults: NNE-SSW sinistral faults such as the Al-Idrisi fault, or NE-SW
faults such as the Carboneras fault, and NW-ESE dextral faults such as the Yusuf fault. The maximum magnitudes recorded
in the Alboran Sea have lower values. Also, the seismic activity in the Alboran Sea is interconnected with the activity in the
southern Iberian Peninsula through the complex tectonic system running E-W from the Rif and Alboran Ridge, Eastern
120 Alboran Basin, to the Arzew faults and alpine Tell chain (e.g., Mourabit et al., 2014; Leprêtre et al., 2018).

Many recorded earthquakes have shallow foci ($h < 50$ km; IGN catalogue), although a significant number of earthquakes
are also generated at intermediate depth (50 - 200 km) and some occur at great depth (600 - 670 km). Deep earthquakes are
in the province of Granada (south of Dúrcal-Alborán Sea) (Molina Palacios, 1998; Buforn and Udías, 2007). Intermediate
seismicity is mainly located in the areas of the Gulf of Cádiz, mainly located within the crust up to a depth of 100 km; about
125 90% of the observed seismicity occurs at approximate depths up to 55-60 km in the Gorringe Bank, High Atlas and in the
Granada-Málaga-O of Alboran area. In the Alboran Sea there is also significant shallow seismicity at depths of less than 30
km, especially in the active Betic-Alboran-Rif shear zone; from here onwards to the W it becomes much deeper.

3. Materials

3.1 Ocean and land digital terrain models

130 The mid-resolution digital terrain model (DTM) employed in this study was constructed after the gridded data set
developed by the four Regional Centres of the Nippon Foundation-GEBCO Seabed 2030 Project (Mayer et al., 2018;
GEBCO Compilation Group 2022, 2022) using satellite altimetry from the European Marine Observation and Data Network
(EMODnet; <http://www.emodnet.eu/>). This global terrain model for ocean and land has a spatial resolution of 15 arc

seconds. The vertical component that the DTM incorporates, for each point over which the hazard is assessed, is used in the
135 estimation of the relative distances, from the site to the seismogenic source, used by some of the GMPEs.

The open source DTM downloaded from EMODnet web site has been resampled by averaging to 0.1° grid resolution, corresponding to cells with approximately 10 km in latitude (Fig. 1) to simplify the comparison of our work with previous studies. Computationally, our estimated PGA using the improved DSHA was performed on a grid of 4,143 sites, generated from the above resampled. This grid size was chosen on the basis of experience and approximately equal to the standard
140 error in earthquake epicentre determination (Panza et al., 1990; Suhadolc, 1990).

3.2 Seismogenic Source Catalogues and Seismicity Parameters

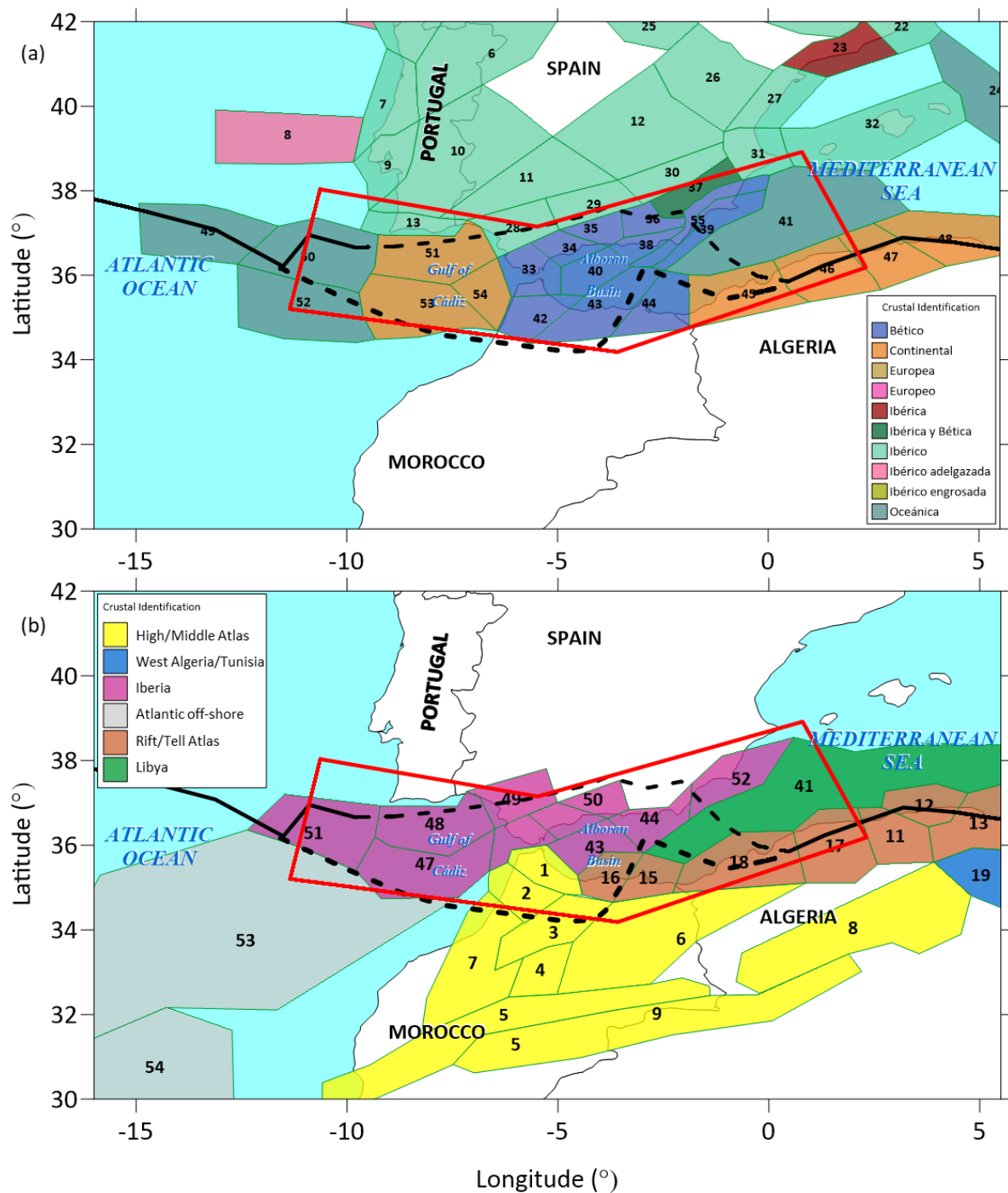
Several seismogenic zonation models partially cover the study area (Table 2). However, there is no single seismogenic zonation that fully covers the area of interest and surrounding areas to effectively account for their effects (Fig. 2). Thus, in this study we opted to integrate different models into an areal seismogenic zonation model covering our studied region,
145 analysing their compatibility. Among the previous seismic zonation models, the selected models, together with their corresponding characteristic seismic parameters, were the ZESIS (Fig. 2a) and the NAF model proposed by Poggi et al. (2020) (Fig. 2b). These models were chosen because the ZESIS model has been used in the SHA for Spain and the NAF is the most recent model for the North African area. Additionally, both models cover geographically and almost entirely overlapping the study area of this work. Initially, the areal seismogenic sources within the limit (perimeter marked in red in
150 Fig. 2) in both models were considered of interest. By integrating both models, the NAF in the north can be complemented with the ZESIS, and the ZESIS east in the south with the NAF.

Table 2: Seismogenic zonation models partially covering the study area.

Zonation model	Covered extension	Reference	Implementation
ZESIS or COMMISSION	Iberian Peninsula	García Mayordomo (2015)	Seismic hazard map of Spain
SA and SB	Portugal	Vilanova and Fonseca (2007)	Seismic hazard map of Portugal
EC8 and ERSTA	Portugal	Carvalho and Malfeito (2018)	Seismic hazard map of Portugal
ESHM13 (SHARE)	Euro-Mediterranean region	Woessner et al. (2015)	Seismic hazard map for Europe
NAF	North Africa	Poggi et al. (2020)	Seismic hazard map of North Africa

4. Seismic hazard assessment

155 Seismic hazard is a concept commonly used to express the probability that the intensity threshold is exceeded, by one or more earthquakes, during the given time period, within a region of interest (McGuire, 2004; Kijko, 2019). It is generally conveyed as a year or multi-year percentage to reach or surpass certain values of peak ground distance, velocity or acceleration, distributed in an area. Seismic hazard is defined in DSHA as the 2nd quartile or other selected percentile (e.g.,



160 **Figure 2.** Seismogenic area zoning in the stable continental crust in the region (SACR). Colours are used to represent the tectonic groups of the SACR: (a) model for South Iberia (modified from ZESIS: IGN-UPM, 2017) and (b) model for North Africa (modified from NAF: Poggi et al., 2020). The number marked in each zone corresponds to its reference in the original zoning ZESIS or NAF model.

84th or 98th as used in this work) of ground motion intensity (PGA measured in g for this work) from a single earthquake or
165 set of earthquakes and is calculated from simple earthquake information and ground motion attenuation relationships
(Krinitzsky, 1995, 2002) that assumes a particular earthquake scenario. Seismic hazard in PSHA is determined by
calculating ground motion frequencies or exceedance rates using a mathematical model based on statistical earthquake (size,
time and location distributions) and ground motion functions (McGuire, 2004, 2008). This model takes into account
uncertainties related to earthquake size and moment (Kramer, 1996). PSHA methods can be categorized into parametric,
170 using the total probability theorem (Cornell, 1968; Kramer, 1996), and nonparametric methods that utilize extreme value
distribution functions (Epstein and Lomnitz, 1966) in SHA. Although both SHA methods use seismological and geological
information, they define and calculate seismic hazard differently, which improves the understanding of seismic hazard
forecasting at the studied site or region (US NRC, 1997; Orozova and Suhadolc, 1999; Wang and Cobb, 2012). The
complementarity and practicality of the DSHA in submerged areas with uncertain and difficult to obtain information are two
175 of the reasons why this work has been chosen as a preliminary SHA alternative to other more complex and data-intensive
hazard assessment methods. A key component of SHAs is the ground motion attenuation equation, which accounts for the
energy loss of the motion due to the distance travelled by the shock. Attenuation models are referred to as ground motion
prediction equations (GMPEs).

180 **4.1 Ground motion prediction equations (GMPEs)**

Attenuation functions are commonly derived from strong ground-motion records for an earthquake (i.e., Campbell and
Bozorgnia, 2003). Functions relate the magnitude M and the distance R of the seismic scenario (M,R). With an appropriate
set of quality records, it is possible to fit a parametric model $f(M,R,\phi_k)$ to estimate the intensity of strong motion (Y) for a
given seismic scenario. The fitted parameters reflect the characteristics of magnitude, and distance scaling, but also near and
185 far -source, faulting mechanism, and hanging wall effects. The heterogeneous geological media causes a dispersion in the
(M,R) sample pairs. So, the correlation between variables can be strong, but never perfect, that means there is an
unavoidable uncertainty or random deviation ε in these regression models. If the expected seismic intensity at the project site
 Y is interpreted as a conditional random variable on the pair (M,R), the fitted model:

$$Y \sim f(M,R,\phi_k) + \varepsilon \quad (1)$$

190 provide an estimate of the median ground motion and the term ε , in terms of magnitude of the earthquake, distance to site,
rupture mechanism and geological conditions (Douglas, 2020). The deviation term ε is identified by a Gaussian distributed
random variable, with null mean $E[\varepsilon]=0$ and variance $\text{Var}[\varepsilon]=\sigma^2$ or random dispersion around the behaviour of the model.

Most GMPEs are defined in terms of finite metrics of relative fault distance to the SHA site assuming a planar rupture geometry. These metrics are usually incorporated in GMPEs as a distance to the surface projection of the rupture so called Joyner-Boore (R_{JB}), or the closest distance to the rupture plane R_{RUP} . However, there are other distances also considered in the GMPEs catalogue formulations where the terms of Eq. (1) involving R distance are given as a function of depth (i.e., R_{RUP}). In these cases, the estimation of the intensity of the motion is affected by the terrain relief (altimetry or bathymetry) where the site is located. Thus, the estimated shake motion Y in mountain areas will be lower than in marine abyssal plains because they are closer to seismogenic sources, and the results of Y estimation in regions with significant unevenness will be sensitive to the use or not of a DTM of the area.

The scarce availability of strong motion records for the whole Ibero-Maghrebian region, drive us to select a representative set of GMPEs, without the possibility of direct comparison with local earthquake records, in a meaningful range for the (M,R) scenarios. Therefore, non-direct selection criteria have to be used, relying on SHA works that has been carried out in the emerged surrounding zones to the study area, and paying special attention to the adequacy of the tectonic context and the suitability of the GMPE functional form (Cotton et al., 2006; Poggi et al., 2020). The fact that the Ibero-Maghrebian study area is a mainly off-shore submarine region geographically located at the confluence of oceanic crust, active continental crust, and stable continental crust complicates the selection of suitable ground motion models. The GMPEs for active tectonic regions strongly underestimate the response spectrum ordinates for western Iberia (Vilanova and Fonseca, 2012). Recent tectonic classifications (Chen et al., 2018; Poggi et al., 2020; Hasterok et al., 2022) describe much of the study region as a Variscan-Hercynian zone in an active shallow crust region (ASCR). This region is surrounded by stable continental cratons in the central African area to the south and the central Iberian Peninsula to the north, and by a stable Atlantic Oceanic region to the west. Hence, it is assumed that in the ASCR there is a homogeneous behaviour of the crust in the ground motion response to seismic shaking, and the set of GMPEs chosen for the area can be applied uniformly over the whole area without distinction.

Seven GMPEs have been selected (Fig. 3a for the GMPEs in the ASCR) considering the updating works of the seismic hazard maps in Portugal, Spain, and North Africa and the European revisions of the SHARE and GEM-OQ homogenisation projects. The weighting of each GMPE has been adjusted considering that they apply equally over the entire extent of the ASCR, according to the values observed at control cities. The PGA is the seismic intensity Y used in all the GMPE models selected in this work. Two equally weighted models for the stable continental crust region (SCCR) and the ASCR of the North African zone: Chiou and Youngs (2008) and Akkar and Bommer (2010) were applied (Poggi et al., 2020). Specifically, the coefficients in AKBO10 from Bommer et al. (2012) have been incorporated and the distance applied in CAFA08 is limited to 15 km, as recommended by GEM-OQ in its inventory of GMPEs (Douglas et al., 2010).

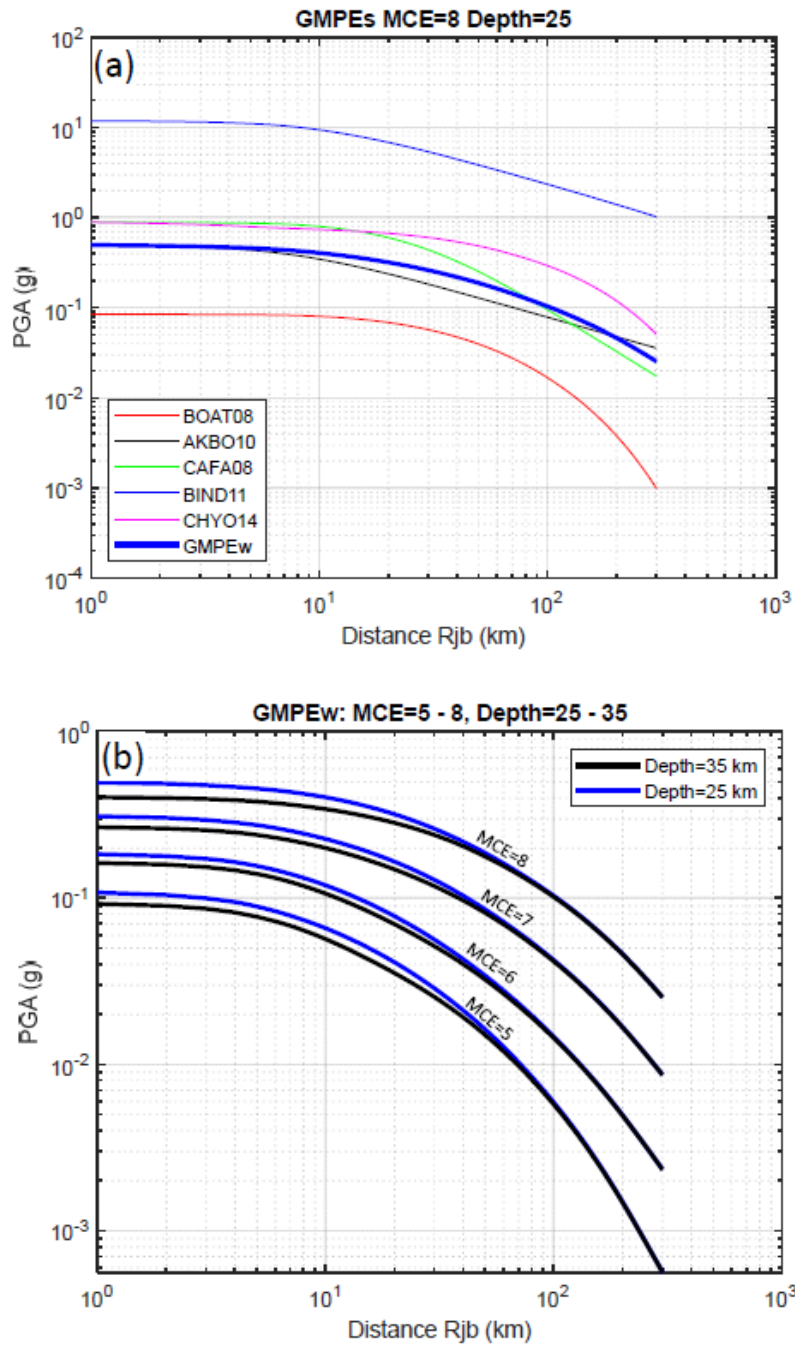


Figure 3. Ground motion prediction equations used, and the resulting weighted composition (GMPEw) applied in this work. (a) GMPEs BOAT08, AKBO10, CAFA08, BIND11 and CHYO14 (for reverse rupture, magnitude Mw 8 and 25 km of source depth). (b) weighted composition of GMPEs for reverse rupture, 25 to 35 km of source depths and Mw range from 5 to 8.

The BOAT08 model (Boore and Atkinson, 2008) has an uncertainty in $\text{Ln}(Y)$ of $\sigma = 0.564$, with Y in g , is valid for the entire magnitude range, uses the R_{JB} distance on its formulation, recommended when the fault geometry is unknown, for focal depths between 2 km and 31 km, and a formulation parameterised according to the focal rupture mechanism (reverse, normal, or rupture-tear). The AKBO10 model (Akkar and Bommer, 2010) has been used in its updated rock version (Bommer et al., 2012), as recommended by GEM-OQ (Giardini et al., 2013; Woessner et al., 2015), to obtain $\log(Y)$, with the PGA in cm/s^2 , considering a formulation in three categories according to the failure mechanism, also using R_{JB} and uncertainties $\sigma_1 = 0.2610$ (intra-event) and $\sigma_2 = 0.0994$ (inter-event). The CAFA08 model (Cauzzi and Faccioli, 2008) provides $\log(Y)$ where Y is in m/s^2 , with an uncertainty of $\sigma = 0.344$ for the horizontal PGA, taking a reference shear wave velocity in the upper 30 m (V_{s30}) of 800 m/s, corresponding to soil type A, according to Eurocode-8 and the R_{JB} distance modified by the depth to the source.

The ECMs in this work are very close to the upper bound of the low magnitudes used in the Spanish hazard model, so the possible effect of the BIND11 model (Bindi et al., 2011) has been considered with an uncertainty of $\sigma = 0.337$, similar to the rest of the models, using R_{JB} to obtain $\log(Y)$, where Y is in cm/s^2 , in rock ($V_{s30} > 800$ m/s) as a function of the different classes of failure mechanisms. The last of the strong shallow ground motion models used is CHYO14 (Chiou and Youngs, 2014), which obtains $\text{Ln}(Y)$, with Y in g in the rock, as a function of the R_{JB} and R_{RUP} distances, for which a value of $Z_{TOR} = 40$ km has been taken as the upper limit of the mean rupture depth, an average dip of 60° , and the different types of rupture mechanisms that act predominantly in each seismogenic area. In this GMPE model, the random variability includes the magnitude dependence with $MCE > 5$ as magnitude threshold, and the nonlinear response of the ground was fitted as a function of V_{s30} (Chiou and Youngs, 2014). Finally, the two GMPE models applied in deep areas are Youngs et al. (1997) and Zhao et al. (2006), correspond with those of the model developed for Spain, based on subduction data or global databases, applied for seismogenic sources at about 60 km depth, three located S and SW of the Gulf of Cádiz and one E of the Strait of Gibraltar, in the Iberian Peninsula (IGN-UPM, 2017). These models are adaptable for scenarios with high magnitudes (up to M_w 8.5) and long distances with slow attenuations, such as those observed in these areas.

250

4.2 Deterministic Seismic Hazard Assessment (DSHA)

The main input parameters in the classic DSHA (Reiter, 1990) are the maximum magnitude associated with the characteristic earthquake as the maximum credible earthquake (MCE) for each seismic source area and a set of attenuation relationship or GMPEs. DSHA does not explicitly incorporate probability and recurrence functions, the seismic hazard can be obtained as a certain percentile of ground motion. The 50th percentile is mostly used in preliminary DSHA studies, as well as the 84th percentile when it is used for critical structures. Thus, some DSHA use the second quartile PGA plus a standard deviation, which is equivalent to an exceedance probability of 16% (Ben-Zion et al., 2003), calculated from simple earthquake and ground motion statistics (Krinitsky, 1995, 2002). To perform these calculations, in this work we follow a

series of steps as the classic DSHA scheme (Reiter, 1990; Krinitzsky, 1995; Kramer, 1996) that allow the deterministic
 260 derivation of the seismic hazard with a zone-based method:

- (i) Build a catalogue of seismogenic sources $\{SS_j\}_{j=1 \dots N_f}$.
- (ii) Assign the seismic potential to each source SS_j with its MCE_j and the prevailing focal mechanism (normal, thrust or strike-slip).
- (iii) Select the set $\{f^i\}$ of the empirical GMPEs or attenuation relationships $Y^i=f^i(M,R,\phi_k^i,\sigma_Y^i)$, with their corresponding
 265 parameters ϕ_k^i and the random uncertainties σ_Y^i for each i-th prediction equation.
- (iv) Arbitrarily select the desired probability of exceedance $PR_{\text{exed}}=\Pr[Y>=y_{\text{max}}/M,R]$, for a seismic scenario given by the (M,R) pair.
- (v) Calculate the p-th percentile equivalent to the probability of exceedance:

$$PC_{Pr}=\Pr[Y<y_p/M,R]=1-\Pr[Y>=y_p/M,R] \quad (2)$$

- 270 (vi) Calculate the standard normal random variable Z_{01} , of mean 0 and variance 1, that matches the percentile PC_{Pr} .
- (vii) Loop for each site P located at the geographic coordinate position (x,y,h) with latitude, longitude and hypsometry (height or depth above mean sea level) do,
- (viii.a) Loop for each j-th seismic source SS_j ($j=1, \dots, N_f$), assuming that the worst-case scenario $(M,R, \text{focal mechanism})$ is selected, defined as the occurrence of an earthquake of magnitude $M=MCE_j$ from a point of the j-th seismogenic source at
 275 the shortest possible distance $R = R_{\text{min}} = \min\{d(P,SS_j)\}$, based on the distance to be handled ($R_{JB}, R_{ep}, R_{hip}, \text{etc.}$) in the attenuation function (Fig. 3).

(viii.a.1) Calculate the median ground motion (50th percentile or GMPE treated as deterministic) of the seismic parameter $Y_{50,j}^i$ at the site, with each i-th GMPE: $Y_{50,j}^i = f^i(M,R,\phi_k^i)$.

(viii.a.2) Calculate the p-th percentile of the seismic parameter at the site with the i-th equation of motion:

$$280 \quad \log Y_{p,j}^i = \log Y_{50,j}^i + Z_{01} \sigma_Y^i \quad (3)$$

(viii.a.3) Obtain the on-site seismic ground shaking parameter $Y_{p,j}$ on site P produced by each j-th earthquake source.

(viii.b) Deterministic evaluation of the th-percentile of the seismic hazard $Y_p(x,y,h)$ at the site located at (x,y,h) as the largest parameter of the intensity of ground shake obtained from each seismogenic source: $Y_p(x,y,h) = \max\{Y_{p,j}\}$

(ix) Write $Y_p(x,y,h)$ output to change to a new location of the P site to assess.

285

However, since in each GMPE the $\log Y$ value is distributed as a normal random variable of mean $\log Y$ with standard deviation σ (Kramer, 1996), and $Y_p(x,y,h) = \max\{Y_{p,j}\}$, both Y_p and $Y_{p,j}$ are random variables. The p-th percentile Y_p is accurately calculated as follows:

$$\Pr[Y_p \leq y_p/M, R] = F\left(\frac{\log Y_p - \log y_{\text{max}}/M,R}{\sigma}\right) = \frac{p}{100} \quad (4)$$

290 in accordance with the classical scheme, with a single dominant seismic source, and where F denotes the cumulative density function of the standard normal distribution (e.g., mean $\mu = 0$, and variance = 1). Now, considering the distribution of $Y_{p,NS}$ as the extreme value of a set of values (Coles, 2001; Ang and Tang, 2007), the above approximation is computed as:

$$\Pr[Y_{p,NS} \leq y_p/M, R] = \Pr[Y_1 \leq y_p/M, R] \times \Pr[Y_2 \leq y_p/M, R] \times \dots \times \Pr[Y_{NS} \leq y_p/M, R] = \frac{p}{100} \quad (5)$$

295 This implies incorporation of the effect of the remaining NS seismic sources in the hazard percentile estimation in the hazard assessment. The estimation is more complicated than in the case of a single source, as it is now necessary to solve the nonlinear equation:

$$\prod_{j=1}^{NS} F\left(\frac{\log Y_{p,NS} - \log y_{j/M,R}}{\sigma}\right) = \frac{p}{100} \quad (6)$$

300 As this paper uses an approach based on a logic tree scheme that weights the GMPEs to capture the epistemic uncertainties in the hazard estimation, the above equation is rewritten to solve for each i-th GMPE $f^i(M,R,\phi_k^i)$ used and its corresponding i-th random uncertainty σ^i :

$$\varphi^i(\log Y_{p,NS}^i) = \prod_{j=1}^{NS} F\left(\frac{\log Y_{p,NS}^i - \log y_{j/M,R}}{\sigma^i}\right) - \frac{p}{100} = 0 \quad (7)$$

from which each $Y_{p,NS}^i$ is obtained.

305

4.3 Epistemic uncertainty treatment: logic tree scheme in DSHA

310 There are numerous uncertainties in the DSHA methodology that arise from a lack of knowledge or limited comprehension of the seismic process. The extreme complexity of the process limits its discernment, which hinders its conceptual understanding for its correct modelling, to its irregular spatial, temporal, and magnitude distribution, to define the seismic sources. In addition, uncertainties arise on the GMPEs, which the statistical adjustment of their coefficients incorporates an estimation error, and arbitrary users choice is itself an unsure process. All these uncertainties can be classified as random and epistemic (McGuire and Shedlock, 1981; Kiureghian and Ditlevsen, 2009).

In this work, we have used a practical method to incorporate the uncertainties inherent in hazard studies that do not have a GMPE developed specifically for the study region, as in our case study, called the logic tree method. Its formulation uses weighting factors assigned to a particular GMPE based on its likelihood (Coppersmith and Youngs, 1986; EPRI, 1987; National Research Council, 1988). An approach to this method can be incorporated into DSHA (Kramer, 1996; Joshi and Sharma, 2008), which has an advantage over the classic scheme in that epistemic uncertainty is better addressed (Bommer et al., 2005; Bommer and Scherbaum, 2008). The logic tree is constructed from a series of branches connected through nodes from which the computational process twigs according to a possibility or appropriate weighting factors $\{w^i\}$, based on expert judgement (Budnitz et al., 1997), depending on the suitability, importance, of a particular GMPE model.

The logic tree used in this study incorporates a combination of seven selected GMPEs to estimate the PGA at the site. The weights assigned to each GMPE in the tree are based on their suitability for different depths of seismic sources. The GMPEs used in this analysis are derived from studies conducted by IGN-UPM (2017) and Poggi et al. (2020) and take into account the specific rupture mechanisms associated with each source. Fig. 3b illustrates the use of our logical tree with various MCEs from sources at different depths. The treatment of uncertainties by the logic tree scheme is made mathematically explicit in the calculation process in the equations to obtain $Y_{p,j}$ at site P produced by each j-th earthquake source:

$$Y_{p,j} = \sum_i w^i Y_{p,j}^i$$

And also, to obtain $Y_{p,NS}$ at each site P:

$$Y_{p,NS} = \sum_i w^i Y_{p,NS}^i$$

which includes the effects of the NS seismic sources. The logic tree scheme shown here is used both for the estimation of the PGA based on a single control source, with the most unfavourable seismic scenario, and for the PGA estimation based on all seismogenic sources with their particular seismic scenario.

4.4 Synthesis of seismogenic zonings

In a considerable extent of the study area, ZESIS and NAF zonings overlap (Fig. 2). The selection of the areal seismogenic sources from both zonings uses here for DSHA was made by taking those that contribute, either by proximity or by maximum magnitude, to the seismicity of the studied area. The seismic influence area was established within a buffer of 300 km (US NRC, 1997) from the study area (Fig. 4a). Additionally, some seismogenic sources adjacent to the area of seismic influence were selected, and their effect was quantitatively studied. Their seismic contribution was analysed by comparing the results obtained from the DSHA with or without these sources.

Geometrically, the overlapping between seismogenic sources, was treated by means of a topological tuning. This operation allowed a geometric adjustment to common perimeters without overlaps (Fig. 4b), considering the seismotectonic

features that control their boundaries. The seismic parameters of each source have also been considered in the synthesis process, as it has been carried out in similar studies (e.g., IBERFAULT, OPPEL, and SISMOGEN projects; García Mayordomo, 2015). Furthermore, the procedure is supported by recent models for classification and segmentation of tectonic regions using fuzzy logic (Chen et al., 2018).

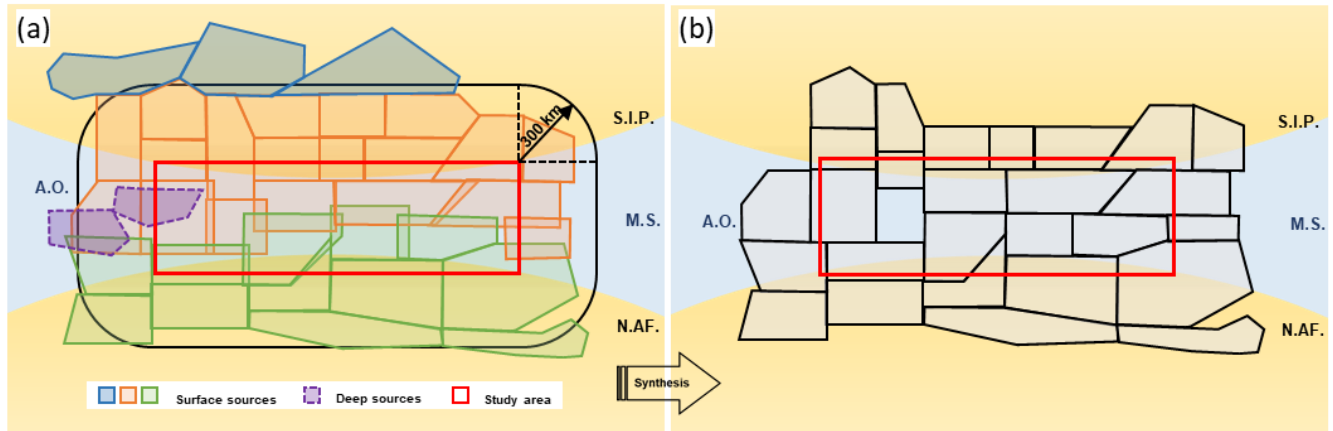


Figure 4. Graphical sketch of: (a) Initial schematic distribution of subsurface and deep seismogenic sources around the study area between the southern Iberian Peninsula (S.I.P.), north Africa (N.AF.), the Atlantic Ocean (A.O.) and the Mediterranean Sea (M.S.), and (b) mapping resulting from the synthesis and integration of seismogenic source zonation from the previous ones.

The MCE values is the seismic characteristic of each seismogenic source as used for DSHA. The estimation of the MCE becomes indispensable as it reflects the maximum energy capacity for a particular seismic source area that can be released in an earthquake. In practice, the MCE is not necessarily the largest magnitude earthquake on the nearest major fault. When geological information is lacking, the MCE is estimated by slightly increasing the historical maximum, usually by one degree in intensity or half a degree in magnitude. However, this adjustment depends on the seismic potential of the specific area. The maximum credible MCE or magnitude of a seismic source is considered to be the upper limit, assuming that no earthquake generated by that source will exceed this magnitude (Joshi and Sharma, 2008). Therefore, the values of the MCEs used in this work for each source resulting from the synthesis have been extracted from the ZESIS (MMmax in Table 10; IGN-UPM, 2017) and NAF (Mmax in Table 7; Poggi et al., 2020) zonings. Although MMmax and Mmax are very similar values or for many sources the same, in others they present slight differences, so $MCE = \max \{MM_{max}, M^{max}\}$ has been taken.

4.5 DSHA calculation specifications

Algorithms to compute a DSHA method have been implemented in varied ways and computer languages (i.e., Ramkrishnan et al. 2021), in MATLAB; Huang and Wang (2012), in IgorPro; Wang et al. (2012), in VBA-Excel). Given some of these codes are open-source available it eases the process of including further improvements. In this paper we have

used the open-source code by Wang et al. (2012) modifying it to incorporate our selection of GMPEs and to account for the logical tree scheme to weight them. This is aiming at considering the relative 3D distances, from a site placed on the DTM (disregarding the curvature of the earth for the dimension of the study area), involved in the formulation of each GMPE. Hence R_x , R_{JB} and R_{RUP} must be reformulated for their calculation (using classic Haversine approximations; Gunawan and Prakoso, 2017). To account for uncertainty in ground motion models, the calculus for each site has evaluated, additionally to the 50%, the effect on DSHA by choosing two values of 16% and 2% of the desired exceedance probability above the mean $PR_{exed} = Pr[Y > y_{max}/M, R]$, for a seismic scenario. In DSHA, the 84th percentile motion to one standard deviation above the mean is usually adopted (Bommer, 2003). The 98th percentile has also been obtained corresponding to the probability of exceedance probability $Pr[Y \leq y_{max}/M, R]$. Last, we considers the DSHA for a specific exceedance probability as the scenario in which all seismic sources contribute (maximum Y distribution in Eq. (5)) and with a logic tree approach (unlike the one used by Wang and Huang (2014), which only work with one GMPE) solving the nonlinear Eq. (7): by means of a numerical Bisection method (halving, binary search, dichotomy or Bolzano method; Atkinson, 1991; Süli and Mayers, 2003). Since this process must be repeated at each site where the hazard is estimated and, in this case, for each GMPE, the convergence characteristics of this algorithm allow it to be repeated for a total of 100 iterations, which are sufficient to achieve an admissible error $|X_o - X^*|$ in the root X^* solution of Eq. (7) (Burden et al., 2015).

4.6 Sensitivity and comparative analyses

Typically, the DSHA is planimetric, and 2D relative source-site distances are evaluated on a horizontal plane. The results obtained with the DSHA method with different exceedance probabilities, as implemented in this work, may be significantly affected by the incorporation of the DTM, as some of the GMPEs use a 3D distance metric in their set of independent variables (e.g., R_{RUP} or R_Y). Likewise, the GMPEs used here incorporate certain rupture type particularities, so that the result of considering the same style in all the sources may give rise to unequal results than if the specific predominant style of each source is used. To assess the sensitivity of the results to the effect of using the DTM and incorporating the information of the rupture style in each source, a descriptive statistical study has been carried out with parametric and nonparametric probabilistic methods on the resulting PGA maps and their absolute differences, with one or all seismic scenarios are used to evaluate PGA.

The PGA maps, obtained by DSHA with DTM and source rupture style, have been tested in two ways: 1) The geographical distribution of PGA values (g) with that obtained and published in four PGA maps (EHSM13-SHARE: Woessner et al. (2015); zoned PSHA: IGN-UPM (2017); unzoned PSHA: Crespo et al. (2014); and NAF zoned PSHA: Poggi et al. (2020)) that partially cover the study area. And 2) Comparing the 50% percentile PGA values obtained from the calculation with the model presented here in nine cities (Fig. 5a) uniformly distributed throughout the study area and for which six previous studies have published their calculated values (in Table 3) of the PGA hazard (Crespo et al., 2014; Rivas Medina, 2014; Salgado Gálvez et al., 2015; Woessner et al., 2015; IGN-UPM, 2017; Poggi et al., 2020).

Table 3: Estimated PGA values (in g) presented from various authors (Annex VI in IGN-UPM (2017), NAF (Poggi et al. 2020), EHSM13-SHARE (Woessner et al., 2015), Crespo et al. (2014), Rivas Medina (2014) and CIMNE (Salgado Gálvez et al., 2015)) in each city used to control the results obtained from the DSHA calculation in the study area.

Main Region	City	Lat.	Long.	IGN-UPM	NAF	EHSM13 SHARE	Crespo	Rivas Medina	CIMNE
Southern Iberian Peninsula	Cádiz	36.533	-6.295	0.11	-	0.10	-	-	-
	Málaga	36.717	-4.424	0.16	-	0.11	-	0.20	-
	Almería	36.836	-2.464	0.19	-	0.13	-	0.30	-
	Huelva	37.267	-6.950	0.12	-	0.13	0.11	-	-
	Granada	37.183	-3.583	0.23	-	0.17	0.30	0.30	0.19
	Alicante	38.200	-0.483	0.18	-	0.11	0.22	0.25	-
North Africa	Tánger	35.791	-5.829	-	0.18	-	-	-	-
	Melilla	35.294	-2.936	-	0.24	-	-	-	-
	Orán	35.708	-0.637	-	0.32	-	-	-	-

405

5. Results

5.1 Seismic zonation

The synthesis and integration of the ZESIS and NAF catalogues over the geographical area in which they overlap within the study area has resulted in a total of 35 zones that form the zonation used in this work (Fig. 5b to d, and Table 4). This zoning incorporates the sources from the NAF to the south and the ZESIS sources within and surrounding the study area. The ZESIS sources to the north (9 to 12, Fig. 2a), on the Iberian crust, have been discarded because of their low influence at the distances marked by the 300 km buffer around it. The constructed catalogue contains, in addition to the geometry of each source, its seismic parameters necessary for the DSHA calculation (Table 4) The depths at which these sources are located vary between 20 and 36 km (Fig. 5b). The seismic characteristics derived from the ASCR seismogenic sources have MCE magnitudes ranging from 6.2 to 8.9 (Fig. 5c). The predominant rupture mechanism is inverse in the band from the Gulf of Cádiz towards the Algerian Mediterranean coast, passing through the southern Rif and running parallel to the Atlas chain (Fig. 5d), which is the characteristic rupture mechanism in areas of plate collision where large compressive stresses act, as in the case of our study region. This mechanism reorganises in the form of shearing toward the Alboran Sea basin and the coastal area of the Iberian Peninsula and towards the interior of the Iberian Peninsula it becomes more extensive with a normal structure. The four deep sources located in the south and southwest of the Iberian Peninsula (between 40 and 65 km depth) were initially and arbitrarily discarded, as they are rejected in the DSHA method when compared, in the search for the maximum PGA, with the seismic scenario of the rest of the ASCR sources at shallower depths.

410
415
420

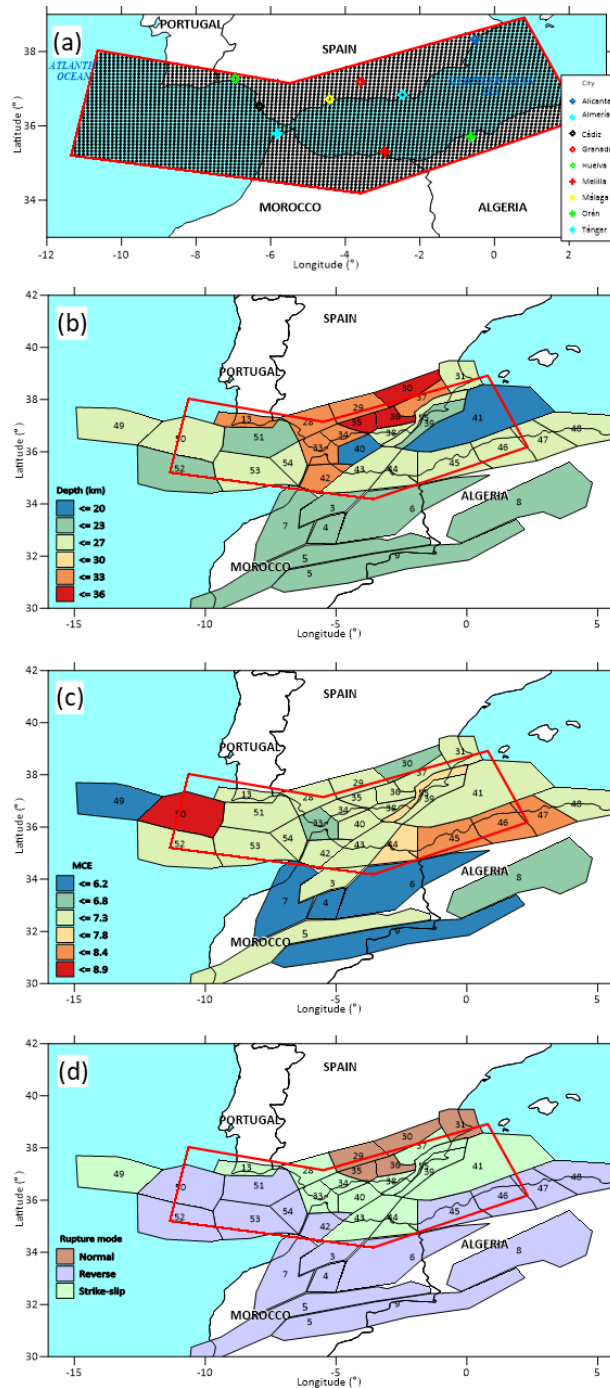


Figure 5. (a) Calculation points (black) and control cities (coloured crosses). Synthesis of the seismogenic source zonation considered in this work for DSHA evaluation on each (a) point, in both South Iberia and North Africa regions and the seismic and geographical distribution parameters (Table 4) used in GMNAFI model for DSHA estimation: (b) depth (km), (c) magnitude of maximum credible earthquake (MCE), and (d) main rupture mechanism for each seismogenic source.

Table 4: Seismogenic sources and their seismic parameters extracted from ZESIS (IGN-UPM, 2017) and NAF (Poggi et al., 2020) zoning models, used for the construction of the synthesis seismogenic model with which the DSHA has been calculated in the study area. The average value MM_{avg} , standard deviation σMM and minimum MM_{min} and maximum MM_{max} truncation limits are parameters of the MCE distribution. MM — Maximum magnitude.

Main Region	Source No. Id.	Rupture Mechanism	Depth (km)	MCE Distribution			
				$\langle MM_{avg} \rangle$	σMM	MM_{min}	MM_{max}
Southern Iberian Peninsula ZESIS	13	Strike-slip	31.0	6.5	0.2	6.0	6.9
	28	Strike-slip	31.0	6.7	0.2	6.3	6.9
	29	Normal	31.0	6.6	0.4	6.2	6.9
	30	Normal	33.0	5.0	0.4	4.6	6.3
	31	Normal	25.0	6.6	0.4	6.5	7.1
	33	Strike-slip	30.0	5.8	0.4	5.4	6.4
	34	Strike-slip	30.0	6.6	0.3	6.3	7.0
	35	Normal	33.0	6.8	0.3	6.5	7.1
	36	Normal	36.0	6.6	0.4	6.2	7.0
	37	Strike-slip	32.0	6.8	0.2	5.4	7.0
	38	Strike-slip	24.0	6.7	0.2	6.5	6.9
	39	Strike-slip	22.0	6.7	0.1	4.9	6.9
	40	Strike-slip	17.0	6.5	0.3	6.0	6.8
	41	Strike-slip	17.0	6.5	0.4	4.7	6.9
	42	Reverse	30.0	6.8	0.3	6.5	7.1
	43	Strike-slip	25.0	7.0	0.2	6.2	7.3
	44	Strike-slip	24.0	6.4	0.4	6.0	7.4
	45	Reverse	26.0	7.3	0.5	6.8	7.9
	46	Reverse	26.0	7.5	0.3	7.2	7.9
	47	Reverse	26.0	7.6	0.4	7.3	8.1
	48	Reverse	26.0	6.8	0.1	6.6	7.1
	49	Strike-slip	24.0	6.0	0.1	5.9	6.2
	50	Reverse	26.0	8.7	0.2	8.5	8.9
	51	Reverse	23.0	6.8	0.3	6.6	7.1
	52	Reverse	23.0	6.4	0.2	6.2	7.1
53	Reverse	24.0	5.7	0.2	5.5	7.0	
54	Reverse	24.0	6.9	0.4	6.5	7.3	
55	Strike-slip	25.0	6.7	0.3	6.6	7.4	
9	Reverse	26.0	6.8	0.3	6.5	7.2	
10	Reverse	31.0	6.3	0.3	5.7	6.8	
11	Reverse	30.0	6.1	0.2	5.9	6.3	
12	Strike-slip	31.0	5.1	0.3	4.9	6.4	
North Africa NAF	3	Reverse	22.0	6.7	0.5	-	7.2
	4	Reverse	22.0	5.2	0.5	-	5.7
	5	Reverse	22.0	6.4	0.5	-	6.9
	6	Reverse	22.0	5.3	0.5	-	5.8
	7	Reverse	22.0	5.5	0.5	-	6.0
	8	Reverse	22.0	5.8	0.5	-	6.3
	9	Reverse	22.0	5.61	0.5	-	6.11

5.2 Seismic hazard maps, sensitivity and quality

The seismic hazard maps PGA (g) obtained (Fig. 6), considering the control scenario at each of the 4,143 points on the map (Fig. 5a), have been obtained for several cases of input data: (i) without using the DTM, assigning 0 m coordinate at each point on the map, and the ASCR seismogenic sources with the same rupture mechanism (inverse, as the most frequent one in Table 4) for all of them (Fig. 6a); (ii) without using the DTM (Fig. 6b), but assigning to each source its particular rupture mechanism (Table 4); (iii) with DTM (Fig. 1) and with the inverse rupture mechanism for all sources (Fig. 6d); and (iv) with DTM and the specific rupture mechanism for each source (Fig. 6e). The maximum PGA values obtained are close to 0.83 g in both cases (PGA(0,reverse) and PGA(0,RM) in Fig. 6c), while the 75th, 50th and 25th percentiles are somewhat lower, in the latter case assigning to each source its rupture style, with a PGA_{50} of about 0.3 g for both. However, using the GEBCO DTM to provide the three-dimensional location for each calculation site, the PGA shows a very modest influence (Fig. 6d and e). PGA values of 1.1 g in both cases (PGA(H,reverse) and PGA(H,RM) in Fig. 6c) are slightly higher than the two previous ones without DTM (Fig. 6a and b), although they do show higher percentile values than the two previous cases (Fig. 6c).

Geographically, the highest PGA values are located on the Gorringe submarine relief up to the Horseshoe plain in all four tested cases. These abyssal areas are affected by sources 50 and 52, with moderate to strong seismicity, which produces PGA outliers in the area, approximately 0.6 g to 0.85 g without DTM and within the values of 0.65 g to 1.1 g with DTM. To the west, the sequence of sources 44 to 47 of moderate seismicity in the Algerian coastal zone in the Arzew faults show values of 0.46 to 0.51 g without DTM, and 0.47 g to 0.54 with DTM. In the case of using a single rupture style, the PGA values show a smooth transition from N to S in the Alborán Sea basin area (Fig. 6a and d), however, when the style specific to each source is applied, this transition is more abrupt (Fig. 6b and e).

Three points (A, B, and C in Fig. 6a) have been selected within the study area to analyze locally in detail the effect of DTM and PGA produced by the surrounding sources according to their relative distance. They are in areas with different seismic conditions in the Gorringe plain, in the Gibraltar Arc, and in the Algerian coastal area. Their elevation has varied from 1000 m above sea level to 4000 m depth to calculate the PGA on each (Fig. 7a). At point A, the PGA increase of up to 17.5% between the result obtained if A were at 0 m (0.83 g) and if A were at 4000 m depth (0.97 g). This increase is reduced to 12.1% for the point C, and in B it is reduced to 10.1%. The effect on the three points can be recognized for all sources within 100 km (Fig. 7b) of relative distance R. There are 4 relevant sources affecting point A (circles), 4 for point B (squares) and three for point C (diamonds), whose PGA are higher than 0.1 g. However, for distances greater than 100 km, there is no difference between using or not using the DTM in the calculation. By observing that the red symbols of A, B and C are superimposed on the blue symbols in Fig. 7b, the PGA values obtained with and without DTM at distances greater than 100 km are very similar and less than 0.1 g.

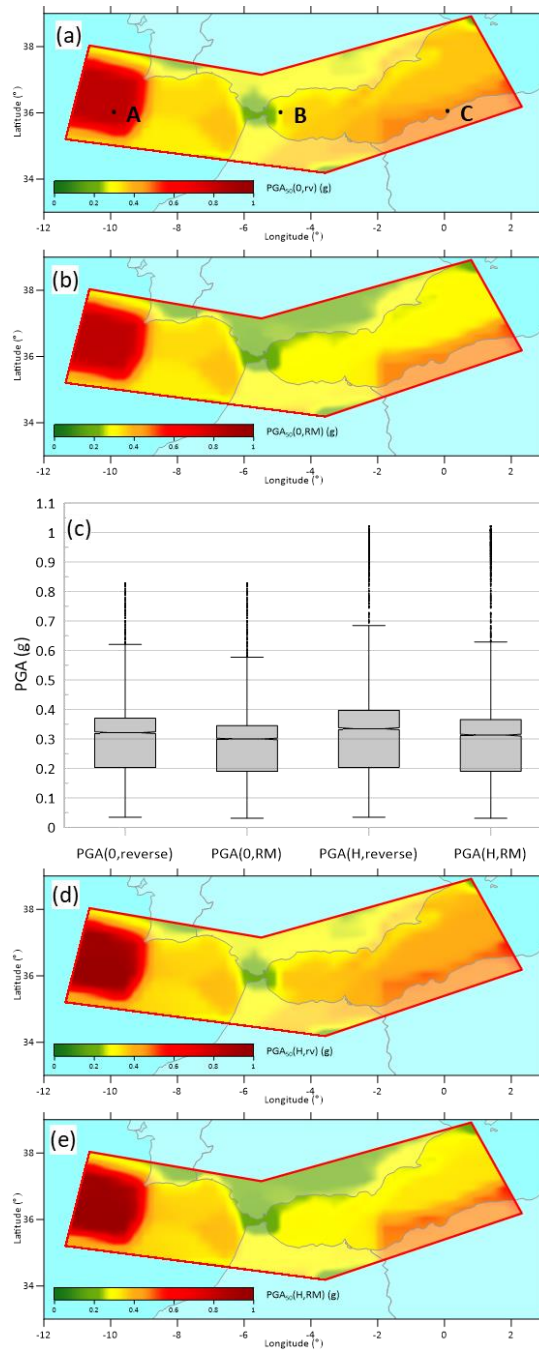


Figure 6. PGA maps from DSHA: (a) without DTM and considering only a reverse rupture mechanism in all seismogenic sources. Probe points A (10°W, 36°N), B (5°W, 36°N) and C (0°E, 36°N) used for sampling PGA map results; (b) without DTM and considering a source-specific average rupture mechanism (Table 4); (c) Box-Whisker plots for PGA values used for Fig. 7a, b, d, and e. Center line represents the mean value. The sample outliers are represented by dot symbols. (d) with DTM (Fig. 1) and considering a reverse rupture mechanism in all seismogenic sources; (e) with DTM (Fig. 1) and considering a source-specific average rupture mechanism (Table 4).

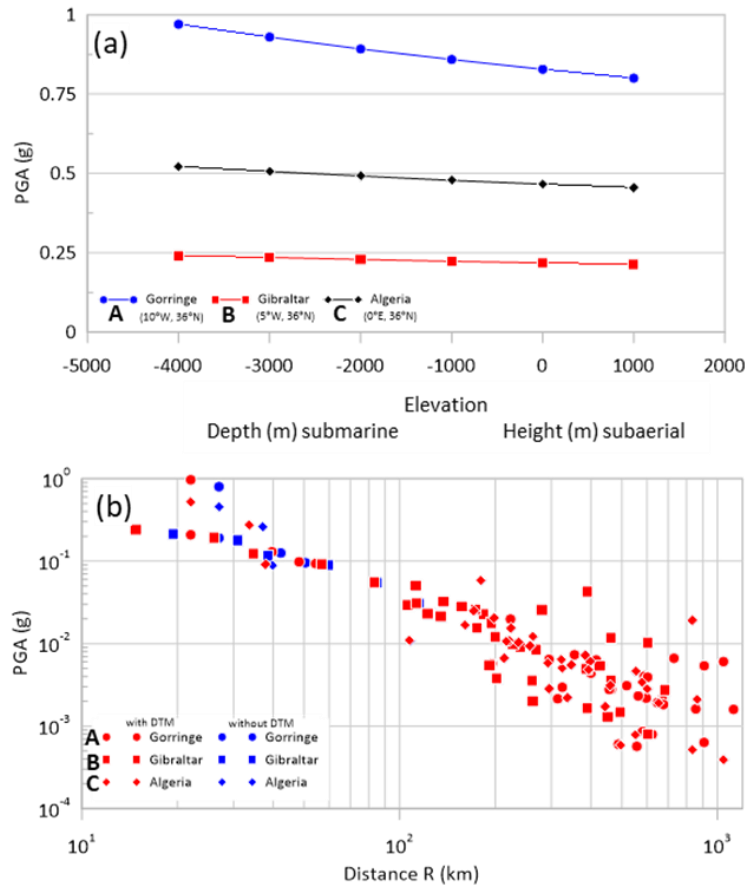


Figure 7. Effect of the DTM on the values obtained at three points distributed in the study area (Fig. 6a): (a) considering that the points are at different elevations and (b) according to the MCE of each source, considering that the points are at 0 m (red symbols, with DTM) and at 475 4000 m depth (blue symbols, without DTM).

Difference PGA maps (in Fig. 8) show that, regardless of whether DTM is used or not (Fig. 8a), the highest difference between assigning or not a predominant rupture mechanism is less than 0.2 g (Fig. 8c). Geographically, the positive increases observed over the reference values calculated without using the DTM (red tones) are areas of the map whose depth is closer to the source, being more intense in the oceanic abyssal plains. So, generally, in submarine areas, the PGA values obtained are higher if the DTM is used (e.g., Gorringe, Horseshoe and Coral Patch areas). The differences are negative (blue shades) in the subaerial areas, although lower than the positive ones (they are below 0.01 g) i.e., the PGA value obtained using the DTM is lower than that obtained without using it. The differences between using a common rupture mechanism according to the predominant one and the specific one of each source do not exceed 0.08 g (Fig. 8b: $PGA(0,reverse)-PGA(0,RM)$ and Fig. 8d: $PGA(H,reverse)-PGA(H,RM)$), highlighting the difference of 0.7 to 0.8 g in the extensional rupture zones (NE of the Betic) and 480 485 PGA(H,reverse)-PGA(H,RM), highlighting the difference of 0.7 to 0.8 g in the extensional rupture zones (NE of the Betic) and with a moderate difference of 0.05 to 0.07 g in the rifting zones distributed in the Alboran basin and East of the Rif.

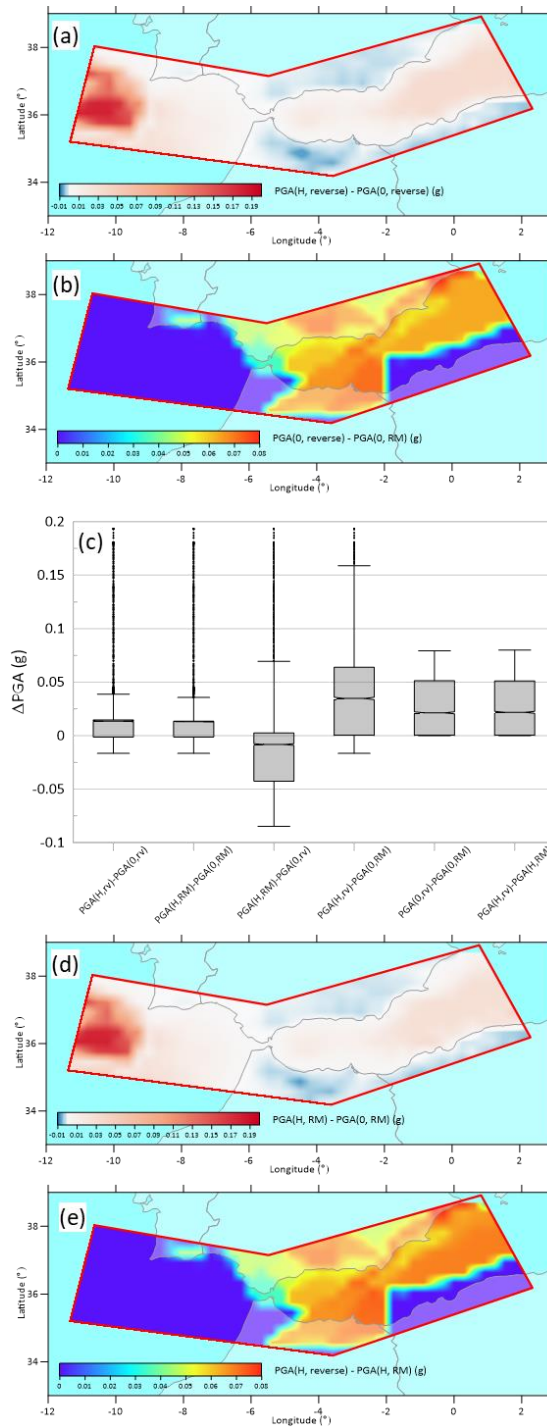


Figure 8. Difference maps between DSHA results in PGA from Fig. 6. Substraction: (a) between Fig. 6d and a; (b) between Fig. 6a and b; 490 (c) Box-Whisker plots for PGA differences used for Figs. 8a, b, d, and e. Center line represents the mean value. The sample outliers are represented by dot symbols; (d) difference between Fig. 6e and b; (e) difference between Fig. 7d and e.

The results obtained for PGA (g) in the nine selected point-cities (Table 3) show variations according to the specified information (DTM and rupture mechanism) for their PGA calculation (columns DSHA¹ to DSHA⁴ in Table 5). Some cities show relevant differences of up to 31% in Granada, others show no variation in the calculated PGA, such as Huelva or Oran, although most of them are between 20.8% in Malaga and 23% in Almeria. Despite these point differences, the spatial distribution of the PGA values in the region, compared to the distributions partially covered by previous works (Fig. 9) are very similar to those obtained in this work. Although it is not the purpose of this paper to discuss the compatibility, lateral, and comparative continuity of the presented maps, it is possible to appreciate some differences between them. However, there is a good fit, both regionally as a whole and locally in specific zones, of the results obtained from the DSHA with DTM and source-specific rupture mechanism with the PGA maps obtained by zoned (Fig. 9a, b and d) and non-zoned (Fig. 9c) PSHA probabilistic methods. The best fits are found in areas with high PGA values: Gorringe, Herradura and Coral Patch to the west, Atlas and Algerian coast to the southeast, and Betic mountain range from Malaga to Alicante to the north; as well as in the areas with lower values in the Alboran Sea basin to the east and south of the Gulf of Cádiz.

Table 5: Estimation of PGA (g) at bedrock level by DSHA at each control city and according to the test cases considered in this work: DSHA¹ result without bathymetric DTM and considering a single reverse rupture mechanism equal for all seismogenic sources; DSHA² result without bathymetric DTM and considering a source-specific rupture mechanism (Table 4); DSHA³ result with bathymetric DTM (Fig. 6a) and considering a reverse rupture mechanism in all seismogenic sources; DSHA⁴ result with bathymetric DTM and considering a source-specific rupture mechanism (Table 4); DSHA₈₄⁵ 84th percentile with bathymetric DTM and considering a source-specific rupture mechanism (Table 4); DSHA₉₈⁶ 98th percentile with bathymetric DTM and considering a source-specific rupture mechanism (Table 4); columns 7 to 9 same as 4 to 6, but using the control and all non-control (NS) sources.

Main Region	City	DSHA ¹	DSHA ²	DSHA ³	DSHA ⁴	DSHA ₈₄ ⁵	DSHA ₉₈ ⁶	DSHA ⁷ all NS	DSHA ₈₄ ⁸ all NS	DSHA ₉₈ ⁹ all NS
Southern Iberian Peninsula	Cádiz	0.27	0.22	0.27	0.23	0.43	0.82	0.59	0.79	1.26
	Málaga	0.29	0.24	0.29	0.24	0.46	0.87	0.50	0.48	1.08
	Almería	0.32	0.26	0.32	0.27	0.52	1.01	0.61	0.83	1.33
	Huelva	0.3	0.3	0.3	0.3	0.57	1.10	0.58	0.81	1.31
	Granada	0.29	0.22	0.29	0.22	0.41	0.78	0.49	0.64	0.99
	Alicante	0.38	0.31	0.38	0.31	0.59	1.15	0.59	0.81	1.31
North Africa	Tánger	0.22	0.18	0.22	0.18	0.34	0.65	0.47	0.63	0.99
	Melilla	0.39	0.32	0.39	0.32	0.61	1.18	0.56	0.79	1.31
	Orán	0.47	0.47	0.47	0.47	0.90	1.74	0.59	0.92	1.75

Even the minima of the PGA for the three PGA percentiles have increased, as seen in the small shift to the right of the the
 535 cumulative frequency distribution curves (Fig. 10d).

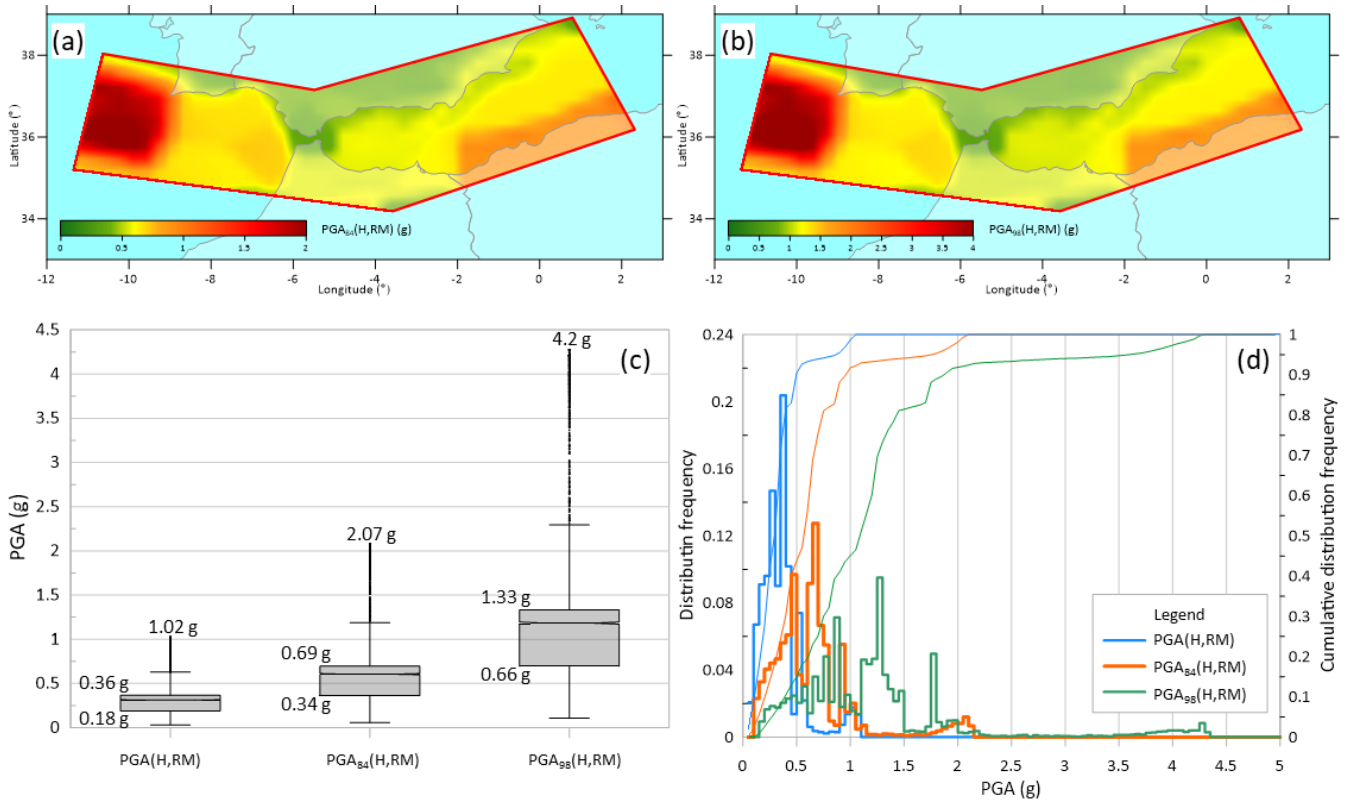


Figure 10. PGA₈₄ (a) and PGA₉₈ (b) hazards maps obtained including the DTM, considering a source-specific average rupture mechanism (Table 4) and random uncertainty for each GMPE. (c) Box-Whisker plots for PGA values in figures (a), (b) and Fig. 6e (for comparison).
 540 Center line represents the mean value. The sample outliers are represented by dot symbols. (d) Histograms, as distribution of relative frequencies, and experimental cumulative distribution functions for PGA values in figures (a), (b) and Fig. 6e (for comparison).

Using the same input data as for the previous exceedance probabilities maps, three new maps have been obtained solving Eq. (7) for each point. As a general result in these three maps (Fig. 11a to c) the joint effect of the 36 seismic sources
 545 a substantial increase in seismic hazard is observed at all points in the study region due to the overall seismic contribution from sources. This geographical distribution reflects the joint nature of the effect of the sources when evaluating the DSHA, increasing by more than 155% in cities such as Cadiz (by 156%) or Tánger (by 161%) for their average GMPEs of 0.59 g and 0.47 g, respectively, when considering all sources in addition to the control source (Table 5, column DSHA⁷ all NS), compared to their average PGA values considering only the control source in the calculation of the DSHA with DTM and a
 550 particular rupture mechanism (Table 5, column DSHA⁴). For the rest of the cities, the effect of the increase in their hazard

values when including all random sources (Table 5, columns DSHA⁷, DSHA₈₄⁸, and DSHA₉₈⁹ all NS) against the comparison PGA averages is between the extreme values indicated, according to the evaluated AMP percentile.

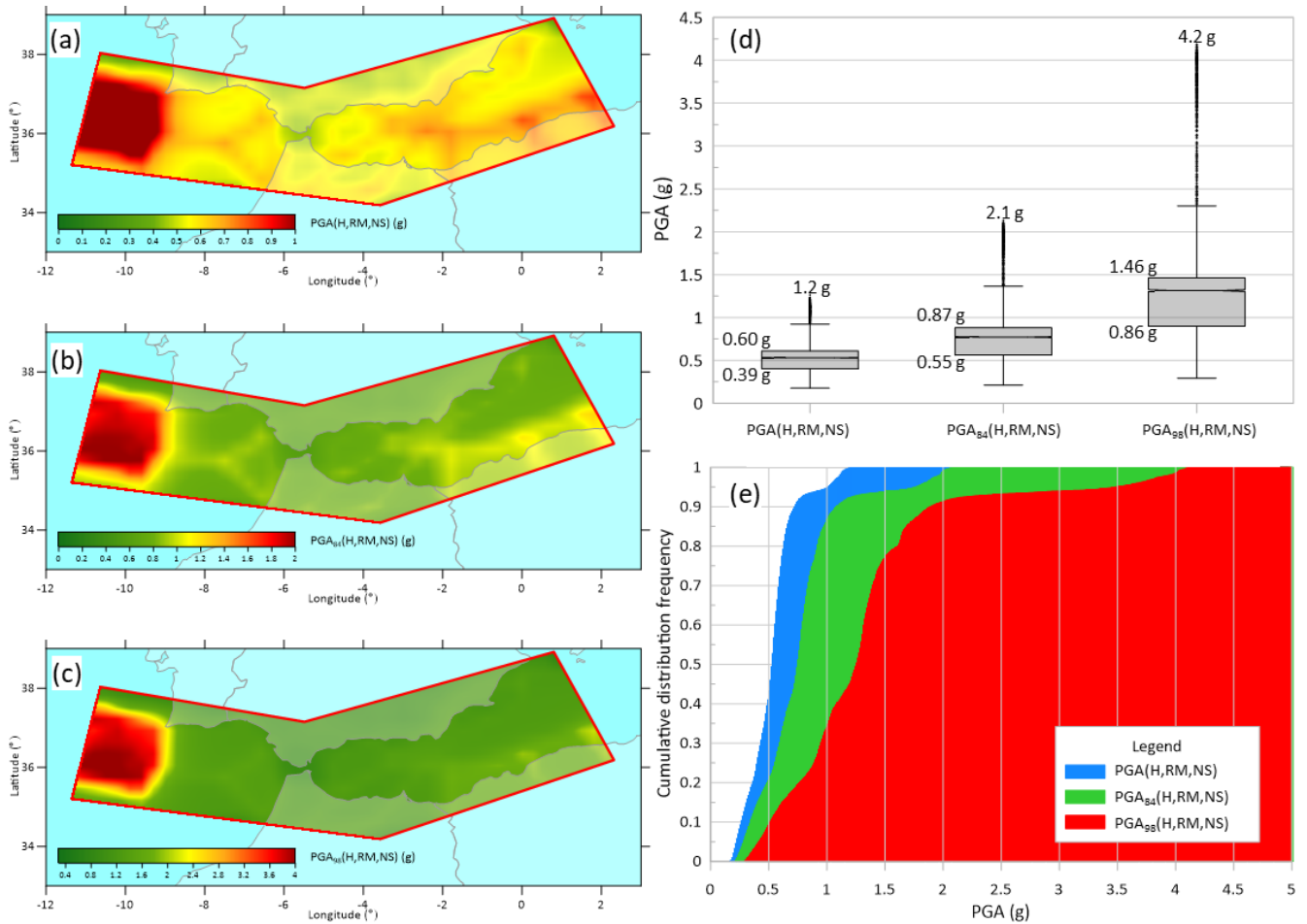


Figure 11. PGA₅₀ (a), PGA₈₄ (b) and PGA₉₈ (c) hazards maps obtained including the DTM, considering a source-specific average rupture mechanism (Table 4), random uncertainty for each GMPE, and cumulative effect on each site of all non-controlling seismogenic sources. (d) Box-Whisker plots for PGA values in (a), (b) and (c). Center line represents the mean value. The sample outliers are represented by dot symbols. (e) Experimental cumulative distribution functions for PGA values in (a), (b) and (c).

6. Discussion

560

Although most seismic hazard analysis studies around the world are presented (i.e., ESHM20_v1 from Pagani et al., 2020) in emerged terrain, the zonings incorporated in the computational models can be used, after an appropriate synthesis and integration process in the areas where they overlap, for seismically active underwater areas. In addition, as the relative

distance from the source to the calculation site is one of the most relevant factors, analyses are more conservative if a DTM
565 is included, which is most noticeable in abyssal active zones. On the other hand, the use of the characterisation of the
predominant rupture mechanism in each seismogenic zone is preferable to using a homogeneous global style for the whole
study area to avoid uniformising the deformation-tectonic stress regime over the entire area. It is preferable to characterize
the rupture mechanism specific to each seismogenic zone instead of applying a uniform style to the entire study area, as this
avoids homogenizing the deformation-tectonic stress regime. The influence of the DTM on the analysis results is more
570 significant in highly seismic areas, whereas the impact is negligible for sources over 100 km away. The differences between
incorporating local seismogenic characteristics from the constructed catalogue and using a DTM are most pronounced in
these distant regions.

Seismic hazard analysis carried out in emerged terrain is useful to provide SHA for underwater areas. Including a DTM,
575 although negligible for emerged land, is relevant for submerged zones and most noticeable in abyssal active zones. On the
other hand, using rupture mechanism in seismic zones is preferable to using a homogeneous global style. The differences
between incorporating local seismogenic characteristics from the constructed catalogue and using a DTM are most
pronounced in these distant regions.

580 The geographical distribution of maximum, minimum, and intermediate PGA values in SHA from previous published
studies with probabilistic methods and partially covering our study area is very similar to the results obtained in this work
with DSHA. This similarity holds true despite using different zonation methods (such as IGN-UPM, 2017; Poggi et al.,
2020) or non-zoned approaches (like Crespo et al., 2014). As Reiter (1990) points out, the DSHA does not contemplate the
inherent uncertainty in the estimation of seismic risk, since the frequency of occurrence and magnitudes are not explicitly
585 considered. So, a less accurate version, distributing the uncertainty due to randomness in the attenuation functions over a
large region, is preferable, even though it provides larger values as in this work. These PGA values can be used as an upper
bound of those that can be achieved, for different exceedance probabilities, such as those applied in this work of 0.16 and
0.02, rather than working with more precise, but less accurate, PGAs.

590 For industrial facilities of important socioeconomic position, where failure consequences are unsustainable, it is
suggested to use the new DSHA to include the seismic hazard from non-controlling sources to ensure that the design is as
safe as possible. Conversely, the conventional DSHA might be suitable for non-critical building or structure designs. In the
study of landslide-triggering hazards that can cause tsunamis, it is important to consider all sources, preferably at the point
event, as noted by Collico et al. (2020). Furthermore, it is crucial to utilize the entire PGA map when applying slope stability
595 methods based on different models, as highlighted by Wang et al. (2021) Wang et al. (2021), to avoid underestimating the
amplitude of the tsunamigenic source, that can have catastrophic consequences for the affected coastline. Therefore, to

ensure accurate assessments and appropriate mitigation measures, it is recommended to account for upper bound uncertainties, as emphasized by Zengaffinen-Morris et al. (2022).

600 The decision for the SHA method is based on its suitability for assessing earthquake hazards, as earthquakes are inherently random and unpredictable. It is important to acknowledge that hazard estimates cannot be fully verified due to the nature of seismic events (Musson, 2012b, a; Wang, 2012). Therefore, the use of DSHA which include the seismic hazard from all sources could be recommended for industrial critical facilities of socioeconomic relevance. Likewise, since underestimating the amplitude of the tsunami wave can have catastrophic consequences on the reached coastline, in the study
605 of earthquake-triggered landslide hazard, it is also relevant to include all sources to produce a conservative PGA map with which to apply slope stability methods (Wang et al., 2021) and evaluate maximum upper bound of displaced water volumes.

7. Conclusions

The assessment of tsunamigenic sources, both seismic and co-seismic submarine landslides, has become a topic of current scientific and technical interest in the context of recent tsunamis. Under these circumstances, seismic hazard analysis
610 in marine areas should become a best practice for assessing coastal tsunami hazard to develop effective coastal inundation prevention and mitigation programmes. However, the analysis of seismic hazard in underwater areas is subject to debate. One reason is that it is typically excluded from national seismic hazard maps as it is not relevant unless there are structures affected by the earthquake. Additionally, there are concerns about the applicability of standard methodologies for assessing seismic hazard in underwater regions. Among these, DSHA also faces this problem. The use of the 50th percentile motion
615 (PGA_{50}) may be insufficient when field evidence indicates that actual seismic motions can sometimes be two (PGA_{84}) or even three standard deviations (PGA_{98}) above the central value, which could lead to seafloor dislocation or a landslide large enough to generate a tsunami.

The results have shown that if the influence of several relevant sources is not fully addressed in the DSHA analysis, it may result in an inadequate SHA, especially when there are numerous sources around the analysed site. In this study we
620 have applied DSHA framework that could arbitrarily consider the controlling seismic source and non-controlling seismic source using extreme likelihood theory to SHA. With this method applied to a submarine region and considering the DTM of bathymetries, a hazard map is presented for the Ibero-Maghrebian marine area, comprised between the western edge of the Gulf of Cádiz and the eastern Mediterranean boundary of the Alboran basin, considering 35 seismogenic sources with their seismic parameters, rupture mode and depth. Compared to the original DHSA, a substantial increase in the intensity of
625 seismic motion is observed, especially at locations close to the confluence of seismic source zones. This acceleration increases as a lower random uncertainty exceedance probability is used. Therefore, this method based on DSHA is suggested to be preliminarily applied in submarine areas, to evaluate the genesis of tsunamis by strong motions triggering possible

large tsunamigenic landslides, making the hazard assessment as safe as possible with the seismic risks provided by each of the seismic sources.

630

Code availability

From the corresponding author upon reasonable request.

Data availability

635 This work used only published or public domain datasets.

Author contributions

AJRB, CPB and MLLI: Investigation. AJRB: literature review. AJRB, CPB and MLLI: conceptualization. AJRB and CPB: methodology. CPB: software. AJRB and CPB: formal analysis. AJRB: writing (original draft). AJRB, CPB and MLLI: writing (review and editing). CPB and MLLI: supervision. MLLI: validation.

640

Competing interests

The authors have no relevant competitive or financial interests to disclose.

Acknowledgements

645 The authors would like to express their gratitude to the reviewers Joao Fonseca and Alexandra Carvalho, whose suggestions helped improve and clarify this manuscript. We would also like to thank Giuliano Panza for his comments. The Open Access publishing for this study has been covered thanks to a CSIC agreement with Copernicus Publications. Thanks to the EMODnet Bathymetry Consortium (2020), EMODnet Digital Bathymetry (DTM). (<https://doi.org/10.12770/bb6a87dd-e579-4036-abe1-e649cea9881a>) to allow the download and use of the current EMODnet DTM version of December 2020, which

650 has a resolution of $1/16 * 1/16$ arc minutes.

References

AEIS-IGN: Seminario sobre criterios sísmicos para centrales nucleares y obras públicas: Madrid, 29-30 de marzo de 1978, Asoc. Esp. Ing. Sísmica AEIS Inst. Geográfico Nac. IGN, 1979.

655 Akkar, S. and Bommer, J. J.: Empirical Equations for the Prediction of PGA, PGV, and Spectral Accelerations in Europe, the Mediterranean Region, and the Middle East, *Seismol. Res. Lett.*, 81, 195–206, <https://doi.org/10.1785/gssrl.81.2.195>, 2010.

- Ang, A. H. and Tang, W. H.: *Probability Concepts in Engineering Planning: Emphasis on Applications to Civil and Environmental Engineering*, John Wiley and Sons, 2007.
- 660 Atkinson, K.: *An Introduction to Numerical Analysis*, John Wiley & Sons, 726 pp., 1991.
- Ayadi, A. and Bezzeghoud, M.: Seismicity of Algeria from 1365 to 2013: Maximum Observed Intensity Map (MOI2014), *Seismol. Res. Lett.*, 86, 236–244, <https://doi.org/10.1785/0220140075>, 2014.
- Ben-Zion, Y., Lee, W. H. K., Kanamori, H., Jennings, P. C., and Kisslinger, C.: Key formulas in earthquake seismology, *Int. Handb. Earthq. Eng. Seismol.*, 81, 1857–1875, 2003.
- 665 Bindi, D., Pacor, F., Luzi, L., Puglia, R., Massa, M., Ameri, G., and Paolucci, R.: Ground motion prediction equations derived from the Italian strong motion database, *Bull. Earthq. Eng.*, 9, 1899–1920, <https://doi.org/10.1007/s10518-011-9313-z>, 2011.
- Bommer, J. J.: Uncertainty about the uncertainty in seismic hazard analysis, *Eng. Geol.*, 70, 165–168, [https://doi.org/10.1016/S0013-7952\(02\)00278-8](https://doi.org/10.1016/S0013-7952(02)00278-8), 2003.
- 670 Bommer, J. J. and Scherbaum, F.: The Use and Misuse of Logic Trees in Probabilistic Seismic Hazard Analysis, *Earthq. Spectra*, 24, 997–1009, <https://doi.org/10.1193/1.2977755>, 2008.
- Bommer, J. J., Scherbaum, F., Bungum, H., Cotton, F., Sabetta, F., and Abrahamson, N. A.: On the Use of Logic Trees for Ground-Motion Prediction Equations in Seismic-Hazard Analysis, *Bull. Seismol. Soc. Am.*, 95, 377–389, <https://doi.org/10.1785/0120040073>, 2005.
- 675 Bommer, J. J., Akkar, S., and Drouet, S.: Extending ground-motion prediction equations for spectral accelerations to higher response frequencies, *Bull. Earthq. Eng.*, 10, 379–399, <https://doi.org/10.1007/s10518-011-9304-0>, 2012.
- Boore, D. M. and Atkinson, G. M.: Ground-Motion Prediction Equations for the Average Horizontal Component of PGA, PGV, and 5%-Damped PSA at Spectral Periods between 0.01 s and 10.0 s, *Earthq. Spectra*, 24, 99–138, <https://doi.org/10.1193/1.2830434>, 2008.
- 680 Budnitz, R. J., Apostolakis, G., and Boore, D. M.: *Recommendations for probabilistic seismic hazard analysis: Guidance on uncertainty and use of experts*, US Nuclear Regulatory Commission (NRC), Washington, DC (United States). Div. of Engineering Technology; Lawrence Livermore National Lab. (LLNL), Livermore, CA (United States); Electric Power Research Inst. (EPRI), Palo Alto, CA (United States); US Department of Energy (USDOE), Washington DC (United States), <https://doi.org/10.2172/479072>, 1997.
- 685 Buforn, E. and Udías, A.: Sismicidad y mecanismo focal de los terremotos de la región Cabo de San Vicente-Argelia, *Rev. Soc. Geológica Esp.*, 20, 301–310, 2007.
- Buforn, E., Sanz de Galdeano, C., and Udías, A.: Seismotectonics of the Ibero-Maghrebian region, *Tectonophysics*, 248, 247–261, [https://doi.org/10.1016/0040-1951\(94\)00276-F](https://doi.org/10.1016/0040-1951(94)00276-F), 1995.
- Buforn, E., Udías, A., and Pro, C.: Large Earthquakes at the Ibero-Maghrebian Region: Basis for an EEWS, *Pure Appl. Geophys.*, 172, 2387–2396, <https://doi.org/10.1007/s00024-014-0954-0>, 2015.
- 690 Buforn, E., Udías, A., and Pro, C.: Source mechanism studies of earthquakes in the Ibero-Maghrebian region and their tectonic implications, *J. Seismol.*, 20, 1075–1088, <https://doi.org/10.1007/s10950-015-9551-7>, 2016.

- Burden, R. L., Faires, J. D., and Burden, A. M.: Numerical Analysis, Cengage Learning, 918 pp., 2015.
- 695 Campbell, K. W. and Bozorgnia, Y.: Updated Near-Source Ground-Motion (Attenuation) Relations for the Horizontal and Vertical Components of Peak Ground Acceleration and Acceleration Response Spectra, *Bull. Seismol. Soc. Am.*, 93, 314–331, <https://doi.org/10.1785/0120020029>, 2003.
- Carvalho, A. M. and Malfeito, N.: Mapas de perigosidade sísmica para Portugal Continental: Uma análise crítica - Parte I – Períodos de recorrência de sismos, 2018.
- 700 Castaños, H. and Lomnitz, C.: PSHA: is it science?, *Eng. Geol.*, 66, 315–317, [https://doi.org/10.1016/S0013-7952\(02\)00039-X](https://doi.org/10.1016/S0013-7952(02)00039-X), 2002.
- Cauzzi, C. and Faccioli, E.: Broadband (0.05 to 20 s) prediction of displacement response spectra based on worldwide digital records, *J. Seismol.*, 12, 453–475, <https://doi.org/10.1007/s10950-008-9098-y>, 2008.
- Chen, Y.-S., Weatherill, G., Pagani, M., and Cotton, F.: A transparent and data-driven global tectonic regionalization model for seismic hazard assessment, *Geophys. J. Int.*, 213, 1263–1280, <https://doi.org/10.1093/gji/ggy005>, 2018.
- 705 Chester, D. K.: The 1755 Lisbon earthquake, *Prog. Phys. Geogr. Earth Environ.*, 25, 363–383, <https://doi.org/10.1177/030913330102500304>, 2001.
- Chiou, B. S.-J. and Youngs, R. R.: Update of the Chiou and Youngs NGA Model for the Average Horizontal Component of Peak Ground Motion and Response Spectra, *Earthq. Spectra*, 30, 1117–1153, <https://doi.org/10.1193/072813EQS219M>, 2014.
- 710 Chiou, B.-J. and Youngs, R. R.: An NGA Model for the Average Horizontal Component of Peak Ground Motion and Response Spectra, *Earthq. Spectra*, 24, 173–215, <https://doi.org/10.1193/1.2894832>, 2008.
- Coles, S.: An Introduction to Statistical Modeling of Extreme Values, Springer, London, <https://doi.org/10.1007/978-1-4471-3675-0>, 2001.
- 715 Collico, S., Arroyo, M., Urgeles, R., Gràcia, E., Devincenzi, M., and Pérez, N.: Probabilistic mapping of earthquake-induced submarine landslide susceptibility in the South-West Iberian margin, *Mar. Geol.*, 429, 106296, <https://doi.org/10.1016/j.margeo.2020.106296>, 2020.
- Coppersmith, K. J. and Youngs, R. R.: Capturing uncertainty in probabilistic seismic hazard assessments within intraplate tectonic environments, in: Proceedings of the Third US national conference on earthquake engineering, 301–312, 1986.
- 720 Cornell, C. A.: Engineering seismic risk analysis, *Bull. Seismol. Soc. Am.*, 58, 1583–1606, <https://doi.org/10.1785/BSSA0580051583>, 1968.
- Cotton, F., Scherbaum, F., Bommer, J. J., and Bungum, H.: Criteria for Selecting and Adjusting Ground-Motion Models for Specific Target Regions: Application to Central Europe and Rock Sites, *J. Seismol.*, 10, 137–156, <https://doi.org/10.1007/s10950-005-9006-7>, 2006.
- 725 Crespo, M. J., Martínez, F., and Martí, J.: Seismic hazard of the Iberian Peninsula: evaluation with kernel functions, *Nat. Hazards Earth Syst. Sci.*, 14, 1309–1323, <https://doi.org/10.5194/nhess-14-1309-2014>, 2014.

- Custódio, S., Lima, V., Vales, D., Cesca, S., and Carrilho, F.: Imaging active faulting in a region of distributed deformation from the joint clustering of focal mechanisms and hypocentres: Application to the Azores–western Mediterranean region, *Tectonophysics*, 676, 70–89, <https://doi.org/10.1016/j.tecto.2016.03.013>, 2016.
- Douglas, J.: Ground motion prediction equations 1964–2020, Dept Civ. Env. Eng Univ Strathclyde Glas. UK, 670, 2020.
- 730 Douglas, J., Faccioli, E., Cotton, F., and Cauzzi, C.: Selection of ground-motion prediction equations for GEM1, GEM Technical Report 2010-E1, GEM Foundation, Pavia, Italy. www.globalquakemodel.org, 2010.
- EPRI: Seismic hazard methodology for the central and eastern United States, Seismicity Own. Group Electr. Power Res. Inst. EPRI, P101-38-45–46, 2256–14, Report NP-472, 1987.
- 735 Epstein, B. and Lomnitz, C.: A Model for the Occurrence of Large Earthquakes, *Nature*, 211, 954–956, <https://doi.org/10.1038/211954b0>, 1966.
- Fonseca, J. F. B. D.: A Reassessment of the Magnitude of the 1755 Lisbon Earthquake, *Bull. Seismol. Soc. Am.*, 110, 1–17, <https://doi.org/10.1785/0120190198>, 2020.
- García Mayordomo, J.: Creación de un modelo de zonas sismogénicas para el cálculo del Mapa de Peligrosidad Sísmica de España, CSIC - Instituto Geológico y Minero de España (IGME), 2015.
- 740 García-Fernández, M., Vaccari, F., Jiménez, M.-J., Magrin, A., Romanelli, F., and Panza, G. F.: Chapter 24 - Regional application of the NDSHA approach for continental seismogenic sources in the Iberian Peninsula, in: *Earthquakes and Sustainable Infrastructure*, edited by: Panza, G. F., Kossobokov, V. G., Laor, E., and De Vivo, B., Elsevier, 491–514, <https://doi.org/10.1016/B978-0-12-823503-4.00006-3>, 2022.
- 745 GEBCO Compilation Group 2022: The GEBCO_2022 Grid - a continuous terrain model of the global oceans and land, NERC EDS Br. Oceanogr. Data Cent. NOC, <https://doi.org/10.5285/e0f0bb80-ab44-2739-e053-6c86abc0289c>, 2022.
- Giardini, D., Woessner, J., Danciu, L., Crowley, H., Cotton, F., Grünthal, G., Pinho, R., Valensise, G., Akkar, S., and Arvidsson, R.: Seismic hazard harmonization in Europe (SHARE): online data resource, *Swiss Seism Serv ETH Zurich Zurich Switz*, 10, 2013.
- 750 Goded, T., Buforn, E., and Muñoz, D.: The 1494 and 1680 Málaga (Southern Spain) Earthquakes, *Seismol. Res. Lett.*, 79, 707–715, <https://doi.org/10.1785/gssrl.79.5.707>, 2008.
- Gonzalez-Castillo, L., Galindo-Zaldivar, J., de Lacy, M. C., Borque, M. J., Martinez-Moreno, F. J., García-Armenteros, J. A., and Gil, A. J.: Active rollback in the Gibraltar Arc: Evidences from CGPS data in the western Betic Cordillera, *Tectonophysics*, 663, 310–321, <https://doi.org/10.1016/j.tecto.2015.03.010>, 2015.
- 755 Grasso, S. and Maugeri, M.: The Seismic Microzonation of the City of Catania (Italy) for the Etna Scenario Earthquake ($M = 6.2$) of 20 February 1818, *Earthq. Spectra*, 28, 573–594, <https://doi.org/10.1193/1.4000013>, 2012.
- Gunawan, P. H. and Prakoso, N. B.: Solution path of Newton’s method for determining epicenter earthquake hazard in Italy 24 august 2016, in: *2017 International Conference on Control, Electronics, Renewable Energy and Communications (ICCREC)*, 2017 International Conference on Control, Electronics, Renewable Energy and Communications (ICCREC), 202–206, <https://doi.org/10.1109/ICCREC.2017.8226707>, 2017.

- 760 Hasterok, D., Halpin, J. A., Collins, A. S., Hand, M., Kreemer, C., Gard, M. G., and Glorie, S.: New Maps of Global Geological Provinces and Tectonic Plates, *Earth-Sci. Rev.*, 231, 104069, <https://doi.org/10.1016/j.earscirev.2022.104069>, 2022.
- Herraz, M., De Vicente, G., Lindo-Ñaupari, R., Giner, J., Simón, J. L., González-Casado, J. M., Vadillo, O., Rodríguez-Pascua, M. A., Cicuéndez, J. I., Casas, A., Cabañas, L., Rincón, P., Cortés, A. L., Ramírez, M., and Lucini, M.: The recent (upper Miocene to Quaternary) and present tectonic stress distributions in the Iberian Peninsula, *Tectonics*, 19, 762–786, <https://doi.org/10.1029/2000TC900006>, 2000.
- 765 Huang, D. and Wang, J.-P.: Seismic hazard map around Taiwan through a catalog-based deterministic approach, in: 15th World Conference on Earthquake Engineering, 2012.
- IGN: Instituto Geográfico Nacional: Geology and tectonics of Gulf of Cadiz, https://www.ign.es/web/resources/sismologia/tproximos/sismotectonica/pag_sismotectonicas/golfocadiz.html, 2023.
- 770 IGN-UPM: Actualización de mapas de peligrosidad sísmica de España 2012, Inst. Geográfico Nac. IGN, 267, <https://doi.org/10.7419/162.05.2017>, 2017.
- Joshi, G. C. and Sharma, M. L.: Uncertainties in the estimation of Mmax, *J. Earth Syst. Sci.*, 117, 671–682, <https://doi.org/10.1007/s12040-008-0063-5>, 2008.
- 775 Kijko, A.: Seismic Hazard, in: *Encyclopedia of Solid Earth Geophysics*, edited by: Gupta, H. K., Springer International Publishing, Cham, 1–14, https://doi.org/10.1007/978-3-030-10475-7_10-1, 2019.
- Kiureghian, A. D. and Ditlevsen, O.: Aleatory or epistemic? Does it matter?, *Struct. Saf.*, 31, 105–112, <https://doi.org/10.1016/j.strusafe.2008.06.020>, 2009.
- Kossobokov, V. and Panza, G.: Seismic roulette: Hazards and risks, *Terra Nova*, 34, 475–494, <https://doi.org/10.1111/ter.12617>, 2022.
- 780 Kramer, S. L.: *Geotechnical Earthquake Engineering*, Prentice-Hall Civ. Eng. Eng. Mech. Ser. Prentice Hall Up. Saddle River, 653, 1996.
- Krinitzsky, E. L.: Deterministic versus probabilistic seismic hazard analysis for critical structures, *Eng. Geol.*, 40, 1–7, [https://doi.org/10.1016/0013-7952\(95\)00031-3](https://doi.org/10.1016/0013-7952(95)00031-3), 1995.
- 785 Krinitzsky, E. L.: How to obtain earthquake ground motions for engineering design, *Eng. Geol.*, 65, 1–16, [https://doi.org/10.1016/S0013-7952\(01\)00098-9](https://doi.org/10.1016/S0013-7952(01)00098-9), 2002.
- Krinitzsky, E. L.: Comment on J.U. Klügel’s “Problems in the application of the SSHAC probability method for assessing earthquake hazards at Swiss nuclear power plants”, in *Engineering Geology*, vol. 78, pp. 285–307, *Eng. Geol.*, 82, 66–68, <https://doi.org/10.1016/j.enggeo.2005.09.004>, 2005.
- 790 Leprêtre, R., Frizon de Lamotte, D., Combier, V., Gimeno-Vives, O., Mohn, G., and Eschard, R.: The Tell-Rif orogenic system (Morocco, Algeria, Tunisia) and the structural heritage of the southern Tethys margin, *BSGF-Earth Sci. Bull.*, 189, 10, <https://doi.org/10.1051/bsgf/2018009>, 2018.
- Loi, D. W., Raghunandan, M. E., and Swamy, V.: Revisiting seismic hazard assessment for Peninsular Malaysia using deterministic and probabilistic approaches, *Nat. Hazards Earth Syst. Sci.*, 18, 2387–2408, <https://doi.org/10.5194/nhess-18-2387-2018>, 2018.
- 795

- López Arroyo, A. and Udías, A.: Aftershock sequence and focal parameters of the February 28, 1969 earthquake of the Azores-Gibraltar fracture zone, *Bull. Seismol. Soc. Am.*, 62, 699–719, <https://doi.org/10.1785/BSSA0620030699>, 1972.
- Martín-Dávila, J. and Pazos, A.: Sismicidad del Golfo de Cadiz y zonas adyacentes, *Física Tierra* ISSN 0214-4557 N° 15 2003 Pags 189-210, 2003.
- 800 Mayer, L., Jakobsson, M., Allen, G., Dorschel, B., Falconer, R., Ferrini, V., Lamarche, G., Snaith, H., and Weatherall, P.: The Nippon Foundation—GEBCO Seabed 2030 Project: The Quest to See the World’s Oceans Completely Mapped by 2030, *Geosciences*, 8, 63, <https://doi.org/10.3390/geosciences8020063>, 2018.
- McGuire, R. K.: Seismic hazard and risk analysis, Earthquake Engineering Research Institute, Berkeley, 2004.
- 805 McGuire, R. K.: Probabilistic seismic hazard analysis: Early history, *Earthq. Eng. Struct. Dyn.*, 37, 329–338, <https://doi.org/10.1002/eqe.765>, 2008.
- McGuire, R. K. and Shedlock, K. M.: Statistical uncertainties in seismic hazard evaluations in the United States, *Bull. Seismol. Soc. Am.*, 71, 1287–1308, <https://doi.org/10.1785/BSSA0710041287>, 1981.
- Mendes-Victor, L. A., Oliveira, C. S., Azevedo, J., and Ribeiro, A.: The 1755 Lisbon Earthquake: Revisited, Springer Netherlands, Dordrecht, <https://doi.org/10.1007/978-1-4020-8609-0>, 2009.
- 810 Molina Palacios, S.: Sismotectónica y peligrosidad sísmica del área de contacto entre Iberia y África, <http://purl.org/dc/dcmitype/Text>, Universidad de Granada, 1998.
- Mostafa, S. I., Abdelhafiez, H. E., and Abd el-aal, A. el-aziz K.: Deterministic scenarios for seismic hazard assessment in Egypt, *J. Afr. Earth Sci.*, 160, 103655, <https://doi.org/10.1016/j.jafrearsci.2019.103655>, 2019.
- 815 Mourabit, T., Abou Elenean, K. M., Ayadi, A., Benouar, D., Ben Suleman, A., Bezzeghoud, M., Cheddadi, A., Chourak, M., ElGabry, M. N., Harbi, A., Hfaiedh, M., Hussein, H. M., Kacem, J., Ksentini, A., Jabour, N., Magrin, A., Maouche, S., Meghraoui, M., Ousadou, F., Panza, G. F., Peresan, A., Romdhane, N., Vaccari, F., and Zuccolo, E.: Neo-deterministic seismic hazard assessment in North Africa, *J. Seismol.*, 18, 301–318, <https://doi.org/10.1007/s10950-013-9375-2>, 2014.
- Musson, R. M. W.: Probability in PSHA: Reply to “Comment on ‘PSHA Validated by Quasi-Observational Means’ by Z. Wang,” *Seismol. Res. Lett.*, 83, 717–719, <https://doi.org/10.1785/0220120036>, 2012a.
- 820 Musson, R. M. W.: PSHA Validated by Quasi Observational Means, *Seismol. Res. Lett.*, 83, 130–134, <https://doi.org/10.1785/gssrl.83.1.130>, 2012b.
- National Research Council: Probabilistic seismic hazard analysis, Natl. Acad. Press Washintong DC, 97 pp., 1988.
- 825 Neres, M., Carafa, M. M. C., Fernandes, R. M. S., Matias, L., Duarte, J. C., Barba, S., and Terrinha, P.: Lithospheric deformation in the Africa-Iberia plate boundary: Improved neotectonic modeling testing a basal-driven Alboran plate, *J. Geophys. Res. Solid Earth*, 121, 6566–6596, <https://doi.org/10.1002/2016JB013012>, 2016.
- Nocquet, J.-M.: Present-day kinematics of the Mediterranean: A comprehensive overview of GPS results, *Tectonophysics*, 579, 220–242, <https://doi.org/10.1016/j.tecto.2012.03.037>, 2012.
- NRC: Reactor site criteria. Appendix a: seismic and geology siting criteria for nuclear power plants, US Nucl. Regul. Comm. NRC Regul. Guide 10CFR100, 1973.

- 830 Orozova, I. M. and Suhadolc, P.: A deterministic–probabilistic approach for seismic hazard assessment, *Tectonophysics*, 312, 191–202, [https://doi.org/10.1016/S0040-1951\(99\)00162-6](https://doi.org/10.1016/S0040-1951(99)00162-6), 1999.
- Pagani, M., Garcia-Pelaez, J., Gee, R., Johnson, K., Poggi, V., Silva, V., Simionato, M., Styron, R., Viganò, D., Danciu, L., Monelli, D., and Weatherill, G.: The 2018 version of the Global Earthquake Model: Hazard component, *Earthq. Spectra*, 36, 226–251, <https://doi.org/10.1177/8755293020931866>, 2020.
- 835 Palano, M., González, P. J., and Fernández, J.: Strain and stress fields along the Gibraltar Orogenic Arc: Constraints on active geodynamics, *Gondwana Res.*, 23, 1071–1088, <https://doi.org/10.1016/j.gr.2012.05.021>, 2013.
- Panza, G. F., Prozorov, A. G., and Suhadolc, P.: Lithosphere structure and statistical properties of seismicity in Italy and surrounding regions, *J. Geodyn.*, 12, 189–215, [https://doi.org/10.1016/0264-3707\(90\)90007-H](https://doi.org/10.1016/0264-3707(90)90007-H), 1990.
- 840 Poggi, V., Garcia-Peláez, J., Styron, R., Pagani, M., and Gee, R.: A probabilistic seismic hazard model for North Africa, *Bull. Earthq. Eng.*, 18, 2917–2951, <https://doi.org/10.1007/s10518-020-00820-4>, 2020.
- Ramkrishnan, R., Kolathayar, S., and Sitharam, T. G.: Probabilistic seismic hazard analysis of North and Central Himalayas using regional ground motion prediction equations, *Bull. Eng. Geol. Environ.*, 80, 8137–8157, <https://doi.org/10.1007/s10064-021-02434-9>, 2021.
- 845 Reilly, W. I., Fredrich, G., Hein, G. W., Landau, H., Almazán, J. L., and Caturla, J. L.: Geodetic determination of crustal deformation across the Strait of Gibraltar, *Geophys. J. Int.*, 111, 391–398, <https://doi.org/10.1111/j.1365-246X.1992.tb00585.x>, 1992.
- Reiter, L.: *Earthquake Hazard Analysis: Issues and Insights*, Columbia University Press, 254 pp., 1990.
- Rivas Medina, A.: *Contribución metodológica para incorporar fallas activas en la modelización de la fuente dirigida a estimaciones de peligrosidad sísmica. Aplicación al sur de España*, phd, E.T.S.I. en Topografía, Geodesia y Cartografía (UPM), 2014.
- 850 Rivas-Medina, A., Benito, B., and Gaspar-Escribano, J. M.: Approach for combining fault and area sources in seismic hazard assessment: application in south-eastern Spain, *Nat. Hazards Earth Syst. Sci.*, 18, 2809–2823, <https://doi.org/10.5194/nhess-18-2809-2018>, 2018.
- 855 Rodriguez, M., Maleuvre, C., Jollivet-Castelot, M., d’Acremont, E., Rabaute, A., Lafosse, M., Ercilla, G., Vázquez, J.-T., Alonso, B., Ammar, A., and Gorini, C.: Tsunamigenic submarine landslides along the Xauen–Tofiño banks in the Alboran Sea (Western Mediterranean Sea), *Geophys. J. Int.*, 209, 266–281, <https://doi.org/10.1093/gji/ggx028>, 2017.
- Sá, L. F., Morales-Esteban, A., and Neyra, P. D.: A deterministic seismic risk macrozonation of Seville, *Arab. J. Geosci.*, 14, 2392, <https://doi.org/10.1007/s12517-021-08626-7>, 2021.
- 860 Salgado Gálvez, M. A., Cardona Arboleda, O. D., Carreño Tibaduiza, M. L., and Barbat Barbat, H. A.: Probabilistic seismic hazard and risk assessment in Spain: national and local level case studies, *Centre Internacional de Mètodes Numèrics en Enginyeria (CIMNE)*, 2015.
- Silva, P. G., Elez, J., Giner-Robles, J., Perez-Lopez, R., Roquero, E., Rodriguez-Pascua, M., Azcárate, T., and Martínez-Graña, A.: *ANÁLISIS GEOLÓGICO DEL TERREMOTO DE TORREVIEJA DE 1829 (ALICANTE, SE ESPAÑA)*, 2019.
- 865 Sinha, R. and Sarkar, R.: Seismic Hazard Assessment of Dhanbad City, India, by deterministic approach, *Nat. Hazards*, 103, 1857–1880, <https://doi.org/10.1007/s11069-020-04059-9>, 2020.

- Soumaya, A., Ben Ayed, N., Rajabi, M., Meghraoui, M., Delvaux, D., Kadri, A., Ziegler, M., Maouche, S., and Braham, A.: Active Faulting Geometry and Stress Pattern Near Complex Strike-Slip Systems Along the Maghreb Region: Constraints on Active Convergence in the Western Mediterranean, *Tectonics*, 37, 3148–3173, <https://doi.org/10.1029/2018TC004983>, 2018.
- 870 Stich, D., Batlló, J., Morales, J., Macià, R., and Dineva, S.: Source parameters of the MW= 6.1 1910 Adra earthquake (southern Spain), *Geophys. J. Int.*, 155, 539–546, <https://doi.org/10.1046/j.1365-246X.2003.02059.x>, 2003.
- Suhadolc, P.: Fault-plane solutions and seismicity around the EGT southern segment, R Freeman St Mueller Ed. Proc. Sixth Workshop Eur. Geotraverse Proj. Eur. Sci. Found. Strasbg., 371–382, 1990.
- Süli, E. and Mayers, D. F.: *An Introduction to Numerical Analysis*, Cambridge University Press, 440 pp., 2003.
- 875 Tahayt, A., Feigl, K. L., Mourabit, T., Rigo, A., Reilinger, R., McClusky, S., Fadil, A., Berthier, E., Dorbath, L., Serroukh, M., Gomez, F., and Ben Sari, D.: The Al Hoceima (Morocco) earthquake of 24 February 2004, analysis and interpretation of data from ENVISAT ASAR and SPOT5 validated by ground-based observations, *Remote Sens. Environ.*, 113, 306–316, <https://doi.org/10.1016/j.rse.2008.09.015>, 2009.
- Udias, A. and Muñoz, D.: The Andalusian earthquake of 25 December 1884, *Tectonophysics*, 53, 291–299, [https://doi.org/10.1016/0040-1951\(79\)90074-X](https://doi.org/10.1016/0040-1951(79)90074-X), 1979.
- 880 US NRC: Identification and characterization of seismic sources and determination of safe shutdown earthquake ground motion, US Nucl. Regul. Comm. NRC Regul. Guide 1165, 1997.
- USCOLD: Committee on Earthquakes. Guidelines for earthquake design and evaluation of structures appurtenant to dams, US Comm. Large Dams USCOLD Denver CO, 75 pp., 1995.
- 885 Vázquez, J. T. (Juan T.), Galindo-Zaldívar, J., Palomino, D. (Desirée), González, L., Fernández-Puga, M. C., Naranjo, S., Pedrosa, M. T., Tintero-Salmerón, V., Bárcenas-Gascón, P. (Patricia), Estrada, F., and Ercilla, G.: SISTEMA DE PLIEGUES ACTIVOS EN EL MARGEN CONTINENTAL SEPTENTRIONAL DEL MAR DE ALBORÁN (MEDITERRANEO OCCIDENTAL), Servicio de Publicaciones de la Universidad de Zaragoza, 2022a.
- Vázquez, J.-T., Ercilla, G., Alonso, B., Peláez, J. A., Palomino, D., León, R., Bárcenas, P., Casas, D., Estrada, F., Fernández-Puga, M. C., Galindo-Zaldívar, J., Henares, J., Llorente, M., Sánchez-Guillamón, O., d’Acremont, E., Ammar, A., Chourak, M., Fernández-Salas, L. M., López-González, N., and Lafuerza, S.: Triggering Mechanisms of Tsunamis in the Gulf of Cadiz and the Alboran Sea: An Overview, in: *Historical Earthquakes, Tsunamis and Archaeology in the Iberian Peninsula*, edited by: Álvarez-Martí-Aguilar, M. and Machuca Prieto, F., Springer Nature, Singapore, 65–104, https://doi.org/10.1007/978-981-19-1979-4_4, 2022b.
- 890 Vilanova, S. P. and Fonseca, J. F. B. D.: Probabilistic Seismic-Hazard Assessment for Portugal, *Bull. Seismol. Soc. Am.*, 97, 1702–1717, <https://doi.org/10.1785/0120050198>, 2007.
- Vilanova, S. P. and Fonseca, J. F. B. D.: Ground-Motion Models for Seismic-Hazard Assessment in Western Iberia: Constraints from Instrumental Data and Intensity Observations, *Bull. Seismol. Soc. Am.*, 102, 169–184, <https://doi.org/10.1785/0120110097>, 2012.
- 900 Wang, J. P. and Huang, D.: Deterministic seismic hazard assessments for Taiwan considering non-controlling seismic sources, *Bull. Eng. Geol. Environ.*, 73, 635–641, <https://doi.org/10.1007/s10064-013-0491-6>, 2014.

- Wang, J.-P., Huang, D., and Yang, Z.: Deterministic seismic hazard map for Taiwan developed using an in-house Excel-based program, *Comput. Geosci.*, 48, 111–116, <https://doi.org/10.1016/j.cageo.2012.05.014>, 2012.
- Wang, Y., Wang, R., and Zhang, J.-M.: Large-scale seismic seafloor stability analysis in the South China Sea, *Ocean Eng.*, 235, 109334, <https://doi.org/10.1016/j.oceaneng.2021.109334>, 2021.
- Wang, Z.: Comment on “PSHA Validated by Quasi Observational Means” by R. M. W. Musson, *Seismol. Res. Lett.*, 83, 714–716, <https://doi.org/10.1785/0220120016>, 2012.
- Wang, Z. and Cobb, J. C.: A critique of probabilistic versus deterministic seismic hazard analysis with special reference to the New Madrid seismic zone, *Recent Adv. North Am. Paleoseismology Neotectonics East Rock.*, 2012.
- 910 Woessner, J., Laurentiu, D., Giardini, D., Crowley, H., Cotton, F., Grünthal, G., Valensise, G., Arvidsson, R., Basili, R., Demircioglu, M. B., Hiemer, S., Meletti, C., Musson, R. W., Rovida, A. N., Sesetyan, K., Stucchi, M., and The SHARE Consortium: The 2013 European Seismic Hazard Model: key components and results, *Bull. Earthq. Eng.*, 13, 3553–3596, <https://doi.org/10.1007/s10518-015-9795-1>, 2015.
- 915 Youngs, R. R., Chiou, S.-J., Silva, W. J., and Humphrey, J. R.: Strong Ground Motion Attenuation Relationships for Subduction Zone Earthquakes, *Seismol. Res. Lett.*, 68, 58–73, <https://doi.org/10.1785/gssrl.68.1.58>, 1997.
- Zengaffinen-Morris, T., Urgeles, R., and Løvholt, F.: On the Inference of Tsunami Uncertainties From Landslide Run-Out Observations, *J. Geophys. Res. Oceans*, 127, e2021JC018033, <https://doi.org/10.1029/2021JC018033>, 2022.
- 920 Zhao, J. X., Zhang, J., Asano, A., Ohno, Y., Oouchi, T., Takahashi, T., Ogawa, H., Irikura, K., Thio, H. K., Somerville, P. G., Fukushima, Y., and Fukushima, Y.: Attenuation Relations of Strong Ground Motion in Japan Using Site Classification Based on Predominant Period, *Bull. Seismol. Soc. Am.*, 96, 898–913, <https://doi.org/10.1785/0120050122>, 2006.